Journal of Materials Chemistry A

REVIEW

View Article Online
View Journal | View Issue

Cite this: J. Mater. Chem. A, 2025, 13, 34055

Electrochemical etching of MXenes: mechanism, challenges and future outlooks

Shaista Nouseen [ab] and Martin Pumera [*abc]

Transition metal carbides, nitrides and carbonitrides, commonly known as MXenes, are an astonishing class of two-dimensional materials, offering versatile surface chemistry, high electrical conductivity, tunable band gaps, and a unique layered morphology, which render them highly attractive for multiple applications ranging from energy storage and conversion to biomedical fields. However, recognising the true potential of MXenes demands precise regulation over their fabrication process and surface functionalization. Traditional MXene fabrication relies on HF acid and fluoride-based etching agents, which pose environmental and safety concerns, subsequently introduce defects and alter surface properties. Consequently, innovative fluoride-free strategies are garnering attention. This review focuses on the eco-friendly electrochemical etching strategy for MXene synthesis, which enriches the MXene surface with a variety of surface terminal groups, such as –O, –OH, and –Cl, varying the electrolyte and etching parameters including their cutting-edge advancements compared to the conventional strategy, highlighting the innovations, challenges, and future outlooks in MXene electrochemical synthesis.

Received 23rd May 2025
Accepted 4th August 2025

DOI: 10.1039/d5ta04176g

rsc.li/materials-a

1. Introduction

Two-dimensional (2D) materials have emerged as an intriguing and groundbreaking class of materials that redefine the limits of conventional materials science.[1–10] There are diverse types of 2D materials such as transition metal dichalcogenides (TMDs),[11] hexagonal boron nitrides,[12–14] graphene,[15–22] phosphorene,[23–25] layered double hydroxides (LDHs)[26,27] and transition metal carbides (MXenes).[28–37] Among other 2D materials, transition metal carbides, commonly known as MXenes, are exceptional 2D materials due to their unique structural morphology, electrical conductivity, larger surface area, tunable band gaps, versatile surface chemistry, and mechanical robustness.[38–50]

MXenes were introduced in 2011 at Drexel University[51] and since then MXenes have been explored for a diverse range of applications, including energy storage,[52–56] like supercapacitors,[57–62] conversion,[63–67] sensing,[68] electromagnetic interference shielding,[69–71] catalysis,[72–74] and in the biomedical field[75,76] (Fig. 1). As the MXene-based electrodes demonstrate few advantages compared to the conventional carbon-based

[a]Quantum Materials Laboratory, 3D Printing & Innovation Hub, Center for Nanorobotics and Machine Intelligence, Department of Chemistry and Biochemistry, Mendel University in Brno, Zemedelska 1, Brno 61300, Czech Republic. E-mail: pumera.research@gmail.com

[b]Future Energy and Innovation Laboratory, Central European Institute of Technology, Brno University of Technology, Purkynova 123, Brno 61200, Czech Republic

[c]Advanced Nanorobots and Multiscale Robotics Laboratory, Faculty of Electrical Engineering and Computer Science, VSB – Technical University of Ostrava, 17. listopadu 2172/15, Ostrava 70800, Czech Republic

Shaista Nouseen is a final year doctoral student at the Department of Chemistry and Biochemistry at Mendel University in Brno, Czech Republic, and a researcher at the Future Energy & Innovation Lab at CEITEC Brno, Czech Republic. She completed her master's degree in applied chemistry from India. Her area of research focus includes the synthesis of 2D nanomaterials, their characterisation, and assembly of 3D-printed electrodes and devices for multiple electrochemical applications such as water splitting, nitrate reduction to ammonia generation, supercapacitors, and batteries.

Martin Pumera has been the Head of the research group at the Future Energy & Innovation Lab at CEITEC Brno, Czech Republic since 2019. He gained his PhD degree in 2001 from Charles University, Prague, Czech Republic. Later, he became a Tenured Group Leader at the National Institute for Materials Science (NIMS), Japan, in 2006, followed by joining Nanyang Technological University, Singapore, as a professor in 2010. His research area varies from quantum materials to 3D printing, electrochemistry, and micro/nanomachines. Martin was given the title of "Highly Cited Researcher" by Clarivate Analytics during the period 2017–2021. Martin published over 950 scientific articles with over 80 000 citations. Martin is proud that 27 of his 125 alumni are group leaders/professor in academia.

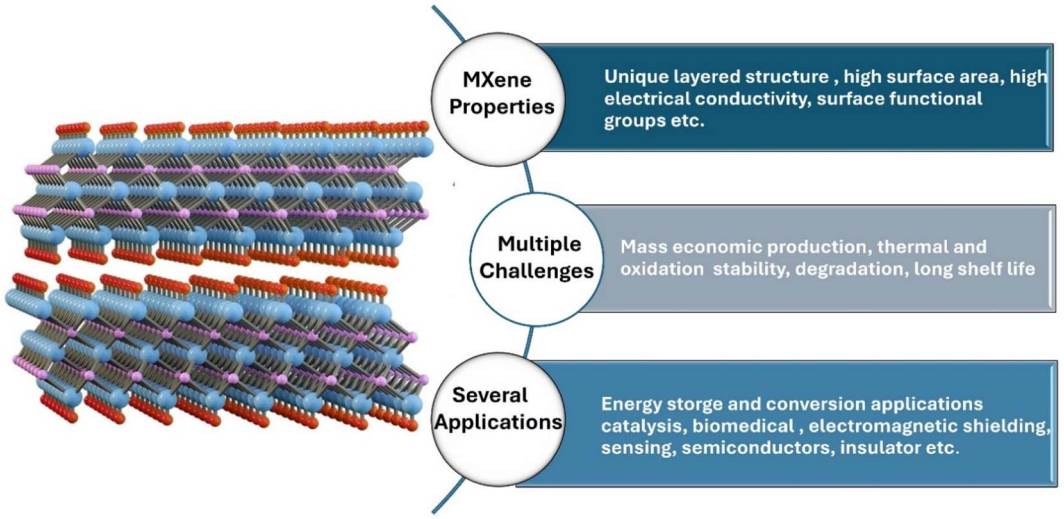

Fig. 1 The MXene properties, multiple applications and wide-ranging applications. MXene structure. Reproduced with permission.[172] Copyright 2021, Wiley-VCH.

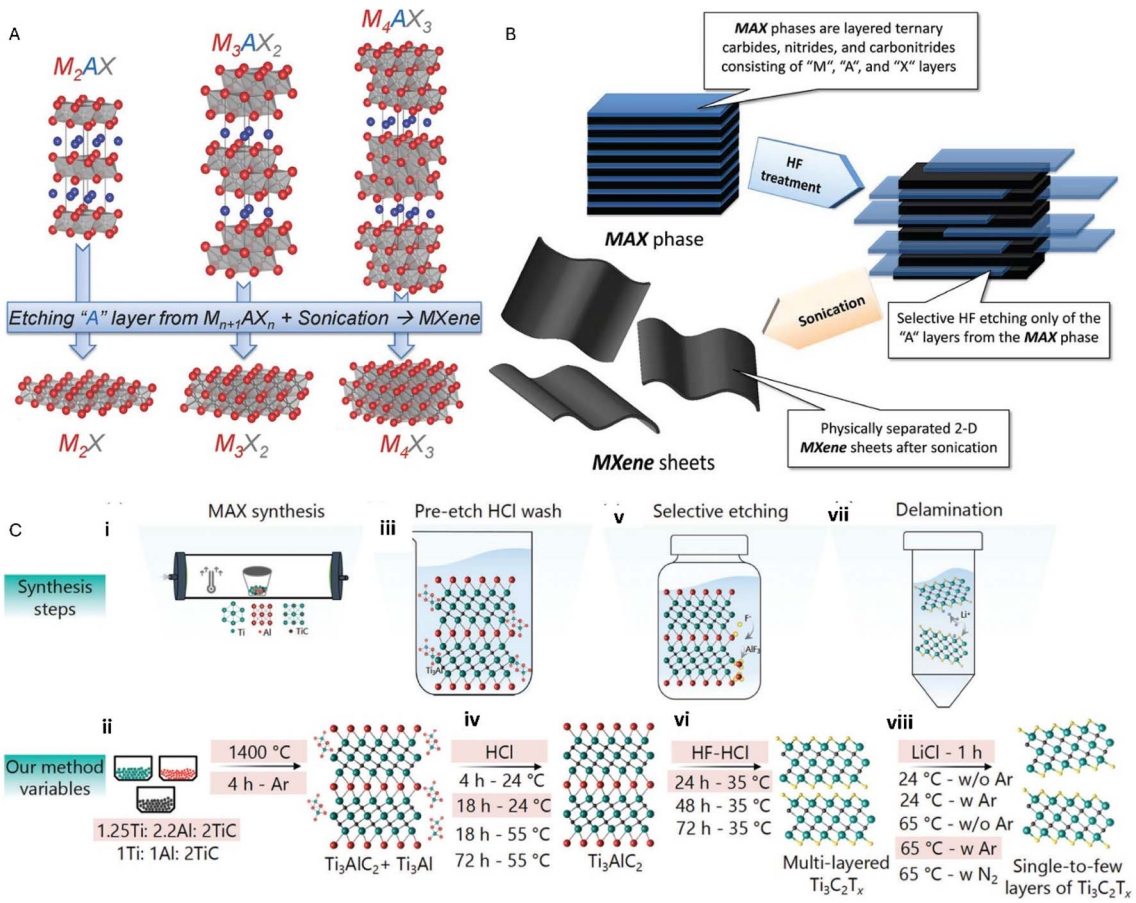

Fig. 2 (A) The illustration of the chemical formula and structure of the MAX phases and their corresponding MXenes. Reproduced with permission.[78] Copyright 2014, Wiley-VCH. (B) The fabrication process of MXene from the corresponding MAX phase *via* HF treatment. Reproduced with permission.[79] Copyright 2012, American Chemical Society. (C) Graphic illustration of the synthesis procedure of the MAX phase and the corresponding MXene. (i) Fabrication of the MAX phase through the reactive pressure-less sintering. (ii) MAX phase fabrication process variables employed in this process. (iii) HCl washing to remove intermetallic impurities. (iv) Pre-etch cleaning of the fabricated MAX phase with HCl by varying the time duration and temperature conditions. (v) The eradication of the aluminium layer from the MAX phase through selective etching. (vi) The etching agent HF–HCl is employed to etch the MAX phase. (vii) Delamination stage to convert the etched multilayered powder into the single-flake MXene. (viii) The delamination variables for the fabrication of the acquired MXene. Reproduced under the terms of the CC-BY license.[80] Copyright 2023, Wiley-VCH.

materials due to their superior conductivity, higher capacitance, and higher energy density, which arise from their unique structure and the ability to combine both electrochemical double layer capacitance (EDLC) and pseudocapacitance, making MXenes ideal for high-performance supercapacitors and energy storage devices.[54,60–62,77]

MXenes are fabricated from their parent ternary layered MAX phases[78] (Fig. 2A). Conventionally, hydrofluoric acid (HF)/HF-based compounds are used to remove the aluminium metal layer from the parent MAX phase[79] (Fig. 2B). Recently, Thakur *et al.* reported the step-by-step fabrication process of MXene,[80] as shown in Fig. 2C. The MXene chemical structure is composed of $M_{n+1}X_nT_x$, where M refers to the number of layers of transition metals ($n = 1, 2, 3,$ or 4), X is represented by carbon and/or nitrogen and T_x is represented by different surface functional groups such as –Cl, –F, –OH, and –O.[81–83] To date, theoretical studies indicate the possibility of different stoichiometric MXenes, and with current progress in the MXene research, the compositions will expand in future.[84–101] MXene family consists of a broad range of promising components, including V_2CT_x, Nb_2CT_x, Mo_2CT_x, Ti_2CT_x, *etc.*[84,85,102–109] To date, the most investigated MXene for multiple applications in the field of batteries,[110–112] supercapacitors,[113–120] electro-photo-catalysis,[121–123] biosensing,[49] and drug delivery[124] among others is titanium-based MXene, *i.e.*, $Ti_3C_2T_x$.[106,125]

However, the main approach for fabricating MXenes is employing HF acid or HF-based compounds as etching agents. The major challenges encountered by employing HF as the etching agent are: (i) the introduction of –F terminal groups on the surface of MXene, which could negatively affect the conductivity and have a detrimental influence on applications such as batteries and supercapacitors.[126–128] (ii) Health hazards for humans occur due to the formation of corrosive and poisonous HF production, as fluoride ions are highly reactive, and extended exposure can easily result in the penetration of fluoride ions into the human body tissue and initiate fatal damage to tissues and organs.[129–133] (iii) The handling of HF requires special personal protective equipment (PPE).[129–133] (iv) The ecological effects due to the formation of corrosive HF are catastrophic for the environment.[130–133] Thus, the requirement to substitute the HF-based compounds for the synthesis of MXene is significant with the non-hazardous, sustainable, and eco-friendly strategies.[134–136]

The MXene synthesis journey began with the revolutionary fabrication of $Ti_3C_2T_x$ (MXene) using the traditional method, which involves employing HF as an etching agent to etch A layers from their parent MAX phases. Subsequently, in 2014, the mixture of hydrochloric acid (HCl) + lithium fluoride (LiF)[137] and later bi-fluoride salts such as $NaHF_2$, NH_4HF_2, KHF_2, NH_4F, *etc.* were employed as etching agents to synthesise MXene, which showcased innovative possibilities.[101,138–143] Moreover, several fluorine-free approaches were explored for MXene fabrication, including the chemical vapour deposition (CVD) method[144] and the electrochemical etching method;[145–151] Jawaid *et al.* reported a halogen etching method to etch the MAX phases to fabricate corresponding MXenes[152] (Fig. 3A); Wang *et al.* reported a HCl-assisted hydrothermal etching approach to fabricate MXenes[153] (Fig. 3B); Wang *et al.* proposed a low-temperature molten-salt (LTMS) etching approach for the fabrication of $Ti_3C_2T_x$ employing NH_4HF_2 as the etching agent[154] (Fig. 3C). Furthermore, trifluoromethanesulfonic acid solution was also employed to synthesise MXenes ($Ti_3C_2T_x$)[155] (Fig. 3D).

Other routes to fabricate MXenes without HF were explored employing HF-free solutions. For example, Shi *et al.* reported an ambient stable iodine-assisted etching method to formulate MXenes[156] (Fig. 4A); Li *et al.* proposed the fabrication of high-purity MXenes through alkali treatment. They etched the MAX phase Ti_3AlC_2 with NaOH in the water solution by varying the etching parameters and etching conditions for the synthesis of fluoride-free-terminated MXene Ti_3C_2 (ref. 157) (Fig. 4B). Liang *et al.* proposed a photo-Fenton approach to fabricate MXenes and compared it to the conventional MXene fabrication process,[158] as shown in Fig. 4C. Several other HF-free routes were reported, including Lewis acid molten salt etching,[159–162] hydrothermal etching,[163] UV-induced selective etching,[164] ball-milling,[165] halogen etching (Br_2, I_2, ICl, IBr, *etc.*),[152] thermal reduction etching,[81] large-scale fabrication of MXene through supercritical etching,[166] and microwave-assisted etching approaches.[167]

Additionally, several MXene hybrid structure formulations were reported using an HF-free based MXene fabrication route, including the fabrication of MXene–copper/cobalt hybrids through the Lewis acidic molten salt etching for excellent energy storage applications in symmetric supercapacitor devices,[168] as illustrated in Fig. 5A. In addition, Huang *et al.* proposed the fabrication of MXene/transition metal sulfide ($Ti_3C_2T_x/MS_y$) heterostructures with interfacial electronic coupling employing a molten salt etching approach. The fabricated $Ti_3C_2T_x/MS_y$ heterostructures were used for sodium storage applications[169] (Fig. 5B). Xuan *et al.* proposed the intercalation and delamination technique for MXene fabrication by treating the Ti_3AlC_2 MAX phase with the organic base tetramethylammonium hydroxide (TMAOH) solution (Fig. 5C), which leads to the formation of $Al(OH)_4^-$-modified and TMA^+-intercalated MXene. The acquired MXene exhibited high NIR absorption. Thus, they were utilised as the photothermal agent against tumour cells.[129] Different types of HF-free etching routes for MXene fabrication, technique, etching agent, terminal groups and their applications are outlined in Table 1.

Among different fluoride-free etching strategies, electrochemical etching is garnering significant research attention due to several benefits such as (i) rapid and selective MXene fabrication with tunable morphology through electrochemical etching of A layers.[170] (ii) A straightforward delamination can be achieved with just sonication in electrochemical capacitors, eliminating the need for multiple steps typically required in the conventional etching method.[171] (iii) Electrochemical etching of MXene with controlled surface termination, which results in improved electrochemical performance.[172] (iv) Green, sustainable, eco-friendly and less hazardous approach compared to HF-based fabrication of MXenes.[172,173] In summary, the main aim of this review is to provide a comprehensive study of the electrochemical etching of MXenes, including an in-depth study to understand the mechanisms and process to selectively remove A layers. Additionally, different transition metal-based MXenes like Ti, Nb, V, and Mo prepared by the electrochemical etching process are discussed. This review article highlights the various advantages of electrochemical etching,

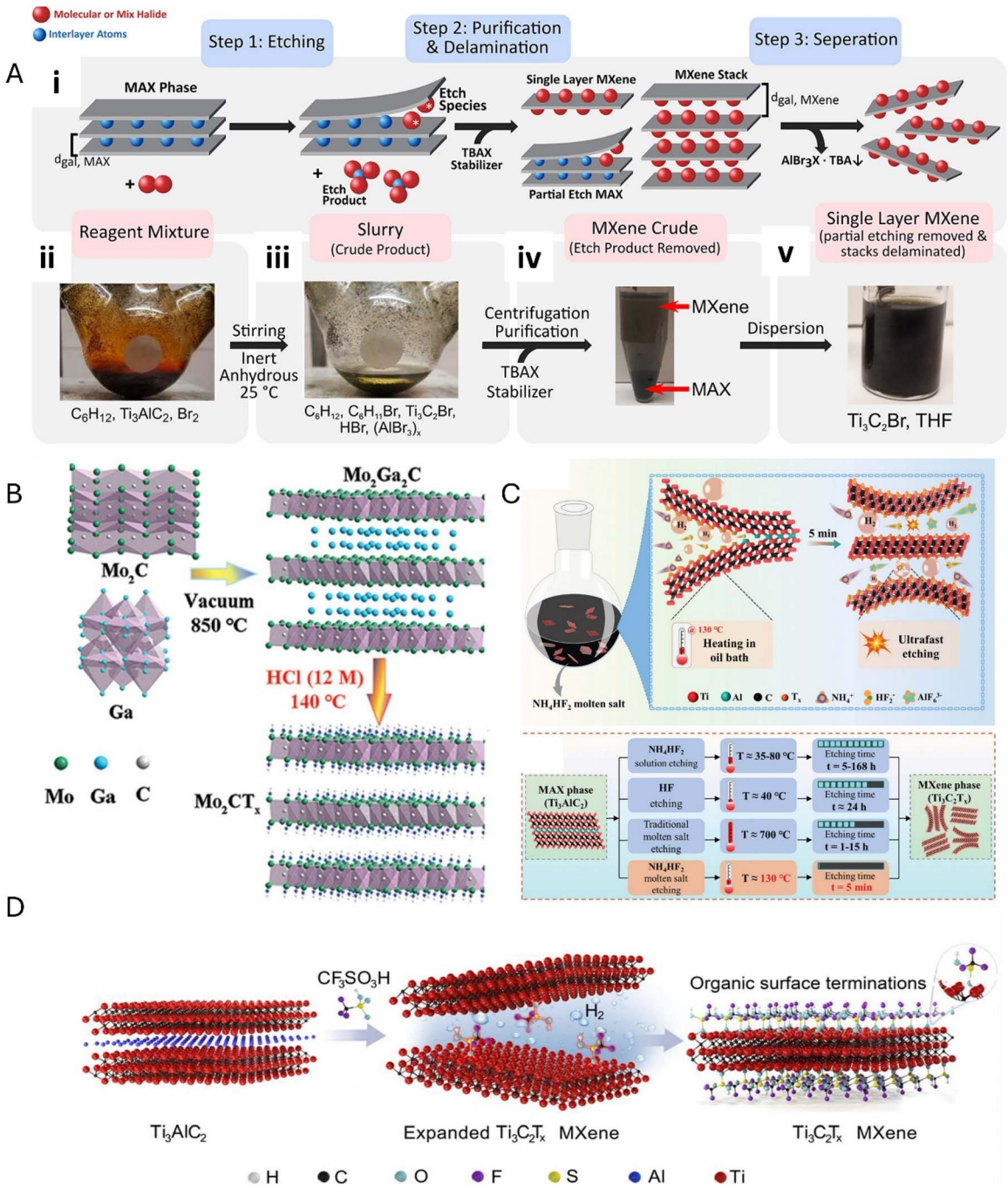

Fig. 3 (A) Schematic illustration of the halogen etching route of the MAX phase to fabricate MXenes. (i) A general procedure of etching, purification, delamination and separation for the creation of halogen-terminated MXenes. (ii) The addition of Br_2 to Ti_3AlC_2 in anhydrous cyclohexane produces a deep red solution. (iii) When bromine (Br_2) reacts with the MAX phase aluminium interlayer, the supernatant solution converts into a pale-yellow coloured solution, indicating the exhaustion of Br_2 in the solution and the creation of the $AlBr_3$ species. $AlBr_3$ species are rendered inert due to the presence of tetrabutylammonium bromide (TBAX), which acts as the stabiliser. (iv) Subsequently, purification of the MXene crude through continual redispersion in the $CHCl_3$ nonpolar solvent. (v) The purified MXene is achieved through dispersion and centrifugation in the THF solvent. Reproduced with permission.[152] Copyright 2021, American Chemical Society. (B) The HF-free Mo_2CT_x MXene was fabricated by employing the HCl-assisted hydrothermal etching approach. Reproduced with permission.[153] Copyright 2021, Wiley-VCH. (C) Diagrammatic representation of the LTMS etching approach to produce the MXene $Ti_3C_2T_x$ employing the NH_4HF_2-LTMS etching method. Reproduced with permission[154] Copyright 2024, Wiley-VCH. (D) Visual representation of the synthesis method of MXene $Ti_3C_2T_x$ from the corresponding MAX phase employing the trifluoromethanesulfonic acid solution. Reproduced with permission.[155] Copyright 2024, Wiley-VCH.

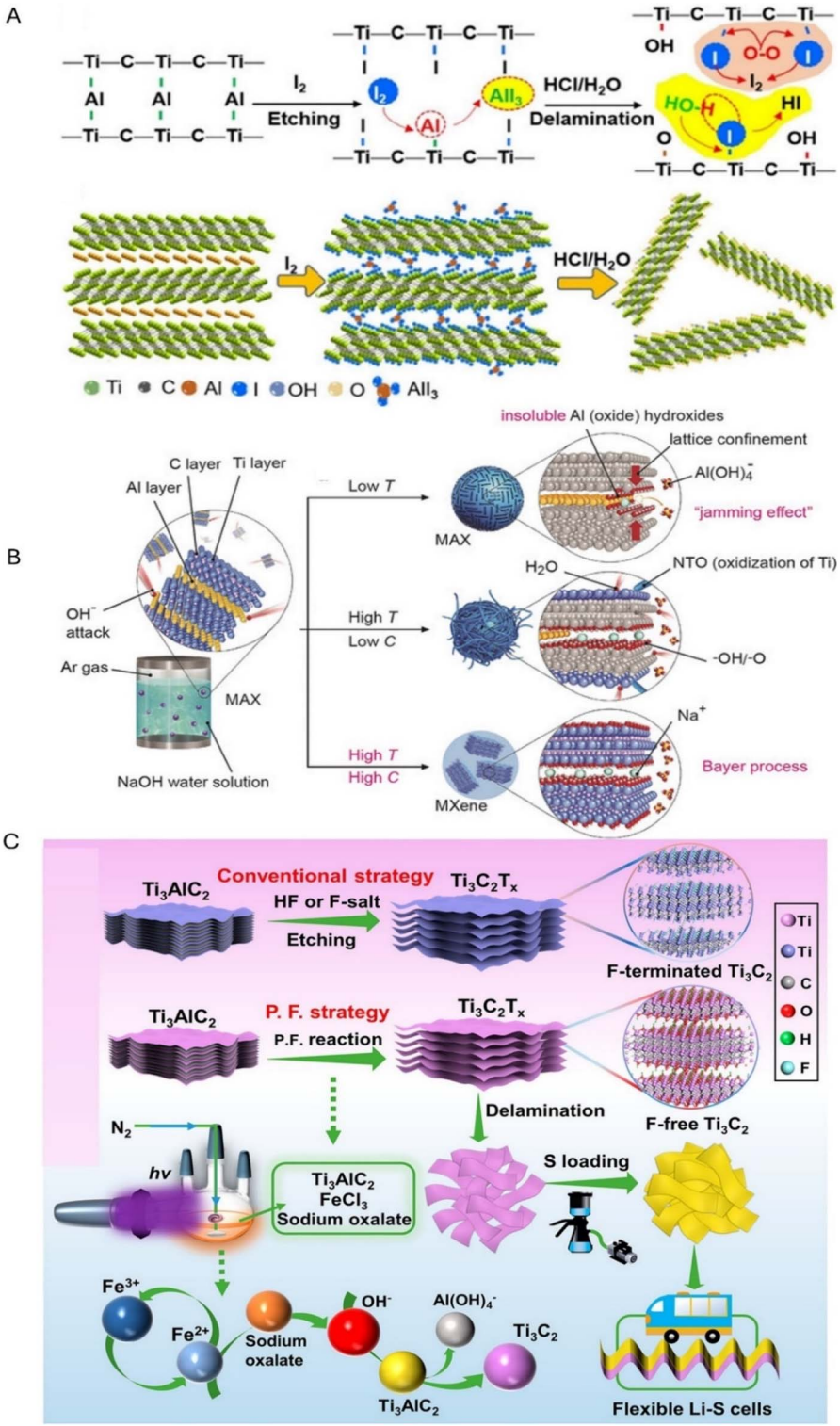

Fig. 4 (A) Schematic illustration of the fabrication and delamination route of the MXene employing iodine-assisted etching. Reproduced with permission.[156] Copyright 2021. Wiley-VCH, under Creative Commons Attribution-NonCommercial-No Derivatives License. (B) Schematic illustration of the fabrication of MXene and the reaction mechanism of etching the MAX phase with NaOH in the water solution by varying etching parameters and conditions. Reproduced with permission.[157] Copyright 2018, Wiley-VCH. (C) Visual illustration of the synthesis of fluoride-terminated MXene Ti_3C_2 through a traditional approach and a graphic model of P. F. approach for the creation of F-free Ti_3C_2 and their application for the flexible lithium–sulfur batteries, along with the diagrammatic representation of the Fe(III)-oxalato P. F. reaction approach. Reproduced with permission.[158] Copyright 2022, American Chemical Society.

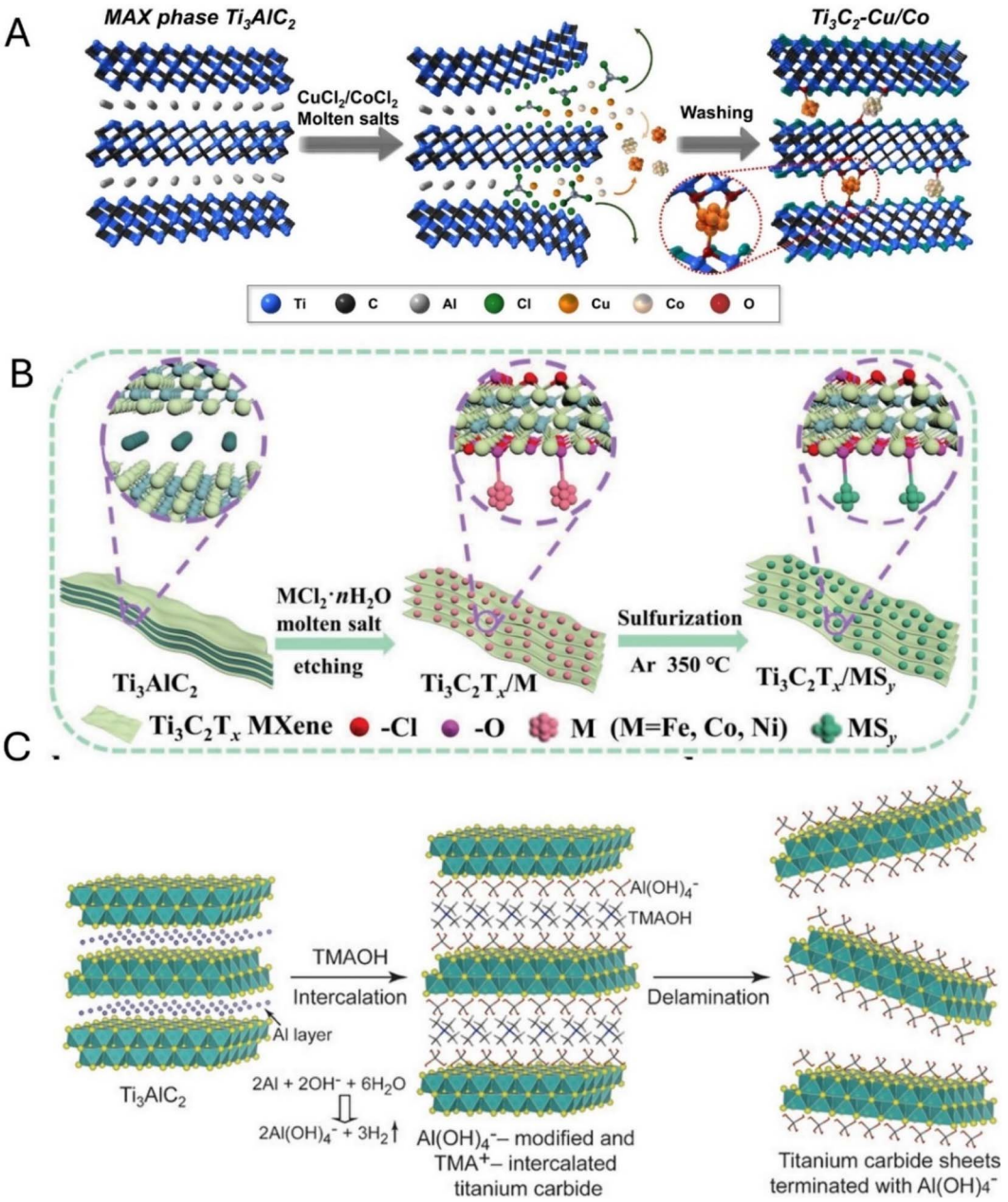

Fig. 5 (A) Schematic illustration of MXene hybrid formulation of Ti_3C_2–Cu/Co. Reproduced with permission.[168] Copyright 2021 Wiley-VCH. (B) A graphic visual of the fabrication procedure of the $Ti_3C_2T_x/MS_y$ heterostructures. Reproduced with permission.[169] Copyright 2022, Wiley-VCH. (C) Graphic demonstration of the intercalation and delamination method for MXene using TMAOH. Reproduced with permission.[129] Copyright 2016, Wiley-VCH.

such as sustainability, cost-effectiveness, and environmental friendliness, compared to the conventional fluoride-based strategies. The innovations, trends, obstacles, and future perspectives in the electrochemical etching of MXene fabrication are briefly discussed (Fig. 6).

2. Mechanism of electrochemical etching

The electrochemical etching approach enables modification of the MXene properties and generates desired patterns/structures on the MXene surface.[192–196] In this approach, MXenes can be synthesised using the corresponding MAX phase as an electrode by selectively etching A layers under a certain applied voltage. Lukatskaya *et al.* employed an electrochemical etching approach using different electrolytic solutions like 5 wt% NaCl, 10 wt% HCl, and 5 wt% HF and MAX as the precursor to fabricate carbon-derived carbon (CDC). They used three different types of MAX phases—Ti_3AlC_2, Ti_2AlC and Ti_3SiC_2. They acquired cyclic voltammetry (CV) profiles, as illustrated in Fig. 7A. In this approach, a certain voltage is applied, which

Table 1 Different HF-free etching routes of MXene fabrication, techniques, etching agents, terminal groups and applications

MXene	Technique	Etching agent	Terminal group	Advantage	Application	Ref
$Ti_3C_2T_x$	Molten salt etching	$CuCl_2$/TBAOH	–Cl	High wettability	Lithium-ion battery	174
$Ti_3C_2T_x$	Molten salt etching	$CuCl_2$/NaCl/KCl	–Cl and –O	High power performance	Electrochemical energy storage	175
$Ti_3C_2T_x$	Molten salt etching	$FeCl_2 \cdot 4H_2O$	–Cl and –O	Remarkably improved electronic conductivity	Sodium storage	169
$Ti_3C_2T_x$	Molten salt etching	$ZnCl_2$	–Cl	Improved electrochemical properties	Sodium-ion battery	176
$Ti_3C_2T_x$	Lewis acid etching	$FeCl_3$	–Cl	Tunable coordination chemistry	Lithium–sulfur batteries	177
$Ti_3C_2T_x$	Lewis acid etching	$ZnCl_2$	–Cl	Element replacement	—	161
$Ti_3C_2T_x$	Lewis acid etching	$CuCl_2$, $CuBr_2$, and CuI_2	–Cl, –Br, and –I	Lattice expansion	Supercapacitor	160
$Ti_3C_2T_x$	Alkali etching	KOH	–OH	Single-layered MXenes	Electrochemical application	178
$Ti_3C_2T_x$	Alkali etching	NaOH	–OH and –O	Larger *c*-lattice parameter	Lithium-ion battery	179
$Ti_3C_2T_x$	Alkali etching	KOH	–OH and –O	Improved catalytic activity	Aerobic oxidative desulfurization	180
$Ti_3C_2T_x$	Hydrothermal alkali etching	NaOH/hydrazine	–OH	—	Nitrate storage	181
$Ti_3C_2T_x$	Hydrothermal alkali etching	NaOH	–OH and –O	High-purity MXene	Supercapacitor	157
$Ti_3C_2T_x$	Hydrothermal alkali etching	NaOH and TMAOH	–OH and –O	MXene nanosheets with a small (∼50–100 nm) lateral size	Nitrogen reduction reaction	182
$Ti_3C_2T_x$	Hydrothermal alkali etching	NaOH	–OH and –O	Resistant to oxidative degradation	Biocompatible	183
$Ta_4C_3T_x$	Acid–alkali etching	HCl/KOH	–OH and –Cl	Biocompatible	Supercapacitor	184
$Ti_3C_2T_x$	Chemical ball-milling etching	LiCl and TMAOH	–OH	Larger surface area	Lithium-ion battery	165
Mo_2CT_x	Microwave-assisted hydrothermal etching	NaOH/Na_2S	–OH and –O	MoS_2/Mo_2CT_x hybrid	Hydrogen evolution reaction	185
$Ti_3C_2T_x$	Organic base etching	TMAOH	–OH and –O	High catalytic activity	Removal of tetracyclic antibiotics	186
Ti_2C–O	Organic base etching	TMAOH	–O	Highly stable	Humidity sensor	187
$Ti_3C_2T_x$	Organic base etching	TMAOH	$Al(OH)_4$	Light absorption in the NIR region	Photothermal therapeutics	129
Mo_2C	Chemical vapour deposition	—	—	Controlled growth of ultrathin 2D Mo_2C crystals on a liquid Cu surface	—	188
Mo_2C	Chemical vapour deposition	—	—	Large area and high quality	—	189
Mo_2CT_x	HCl-assisted hydrothermal etching	HCl	–O and –Cl	High efficiency	Energy storage applications	153
$Ti_3C_2T_x$	Halogen/acid etching	I_2/HCl	–OH and –O	High stability	Supercapacitor	156
$Ti_3C_2T_x$	Halogen/halide etching	IBr, ICl, I_2, Br_2, and TBAX	Halides	Controlled surface chemistries	—	152
Mo_2CT_x	Halide etching	HBr solution, LiBr, NaBr, KBr, and NH_4Br	–Br	Enhanced photocatalytic performance	H_2 production	74
Ti_2CT_x	Thermal reduction	Mixed argon/hydrogen (Ar/H_2, 95/5, v/v) flow temperature between 400 and 900 °C	—	Large-scale MXene production	Lithium-ion storage	81
$Ti_3C_2T_x$	Lithiation expansion	Li foil/LiTFSI	–OH and –O	Rapid and scalable synthesis	Supercapacitor	134
$Ti_3C_2T_x$	Photo-Fenton approach	Sodium oxalate/$FeCl_3$	–OH and –O	High purity with 95% yield	Lithium–sulfur batteries	158
Mo_2CT_x	UV-assisted etching	UV light	—	High purity	Lithium-ion batteries and sodium-ion batteries	164
Mo_2CT_x	UV-assisted phosphoric acid etching	UV light and phosphoric acid	—	Safe etching route	—	190
$Ti_3C_2T_x$	Hydrothermal acidic etching	HCl	–OH, –O or –Cl	Enhanced electrochemical properties	Supercapacitor applications	191

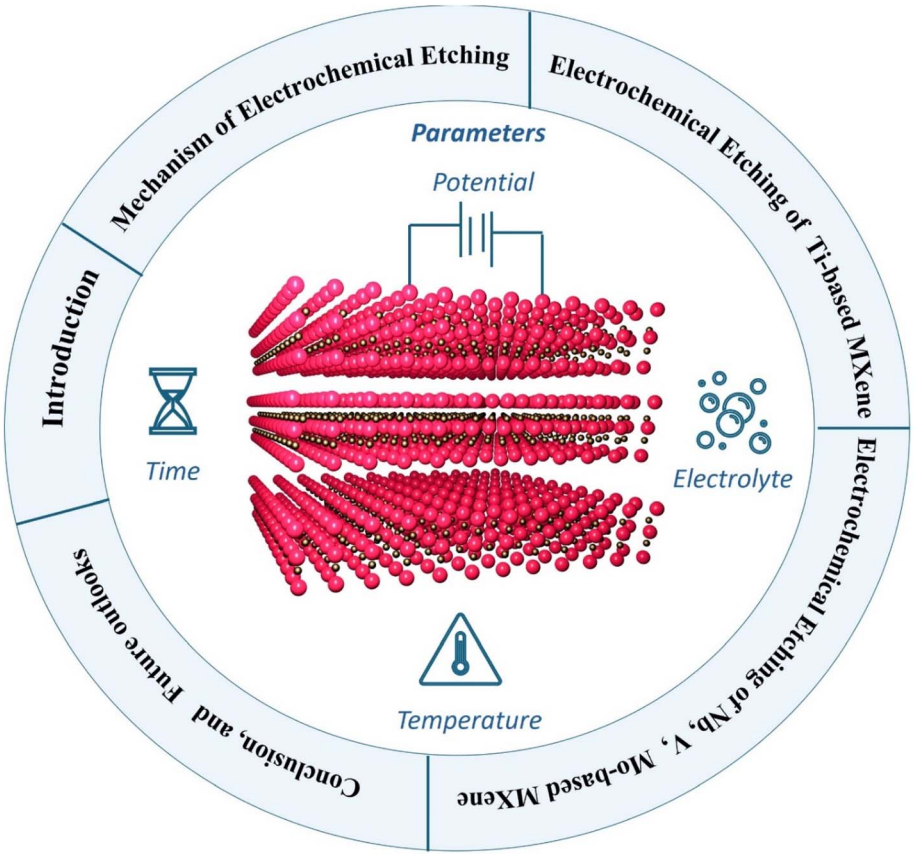

Fig. 6 The outline of the review article.

facilitates the disruption of the M–A bonds in the MAX phase and initiates aluminium layer etching simultaneously.

However, when the voltage rises gradually, it eliminates the transition metal (M) layers, producing amorphous carbon. In summary, this report is crucial for the electrochemical etching of MXene. As it confirms that the regulation of the voltage window and time duration associated with the reaction concerning M and A layers are crucial parameters to selectively eliminate A layers and assist in effective MXene fabrication without the removal of M layers.[197] This method emphasises the importance of the regulation of the etching parameters to obtain optimum conditions for MXene fabrication. Moreover, to better understand the significance of the electrochemical etching parameters, a summary of electrochemical etching techniques, which includes different parameters like electrolytic solution, voltage window, time duration and temperature, is provided in Table 2.

Sun *et al.* first reported an electrochemical etching route to fabricate Ti_2C MXene using the Ti_2AlC porous MAX phase electrodes. In this approach, a controlled potential is provided for the electrochemical etching using diluted aqueous hydrochloric acid (HCl) as an etching agent.[198] The MAX phase Ti_2AlC was cut into pieces ($0.7 \times 3 \times 0.1$ cm^3), and a copper wire was attached to this MAX phase parallelepiped utilising a flash-dry silver paint. To protect the lower part of the copper wire and flash-dry silver paste, an epoxy paste was utilised. In a three-electrode system, cyclic voltammetry profiles were acquired, providing the cycling rate at 20 mV s^{-1}, where the MAX phase parallelepiped acts as the working electrode, Pt foil acts as the counter electrode and Ag/AgCl acts as the reference electrode. After the electrochemical etching procedure, the MAX phase electrodes were rinsed with deionised water to remove the remaining aqueous HCl electrolytes on the electrode surface.

First, in the aqueous HCl electrolyte, the elimination of the aluminium (Al) layers from the Ti_2AlC electrodes occurs, which results in the fabrication of the Ti_2CT_x MXene containing several terminal functional groups like hydroxide (–OH), chloride (–Cl), and oxygen (–O). This reaction mechanism is very similar to the chemical etching of the MAX to MXene using traditional etching approaches, like using HF or LiF/HCl as the etching agent. Subsequently, after the successful elimination of the Al metal from the MAX phase, the functional group –Cl is attached to the surface of the fabricated MXene.[198] The elimination of the Al layer on the MAX phase as the working electrode is shown in eqn (1):

$$Ti_2AlC + yCl^- + (2x + z)H_2O \rightarrow Ti_2C(OH)_{2x}Cl_yO_z + Al^{3+} + (x + z)H_2 + (y + 3)e^- \quad (1)$$

Simultaneously, at the Pt counter electrode, the subsequent reaction is shown in eqn (2):

$$Al^{3+} + 3e^- \rightarrow Al \quad (2)$$

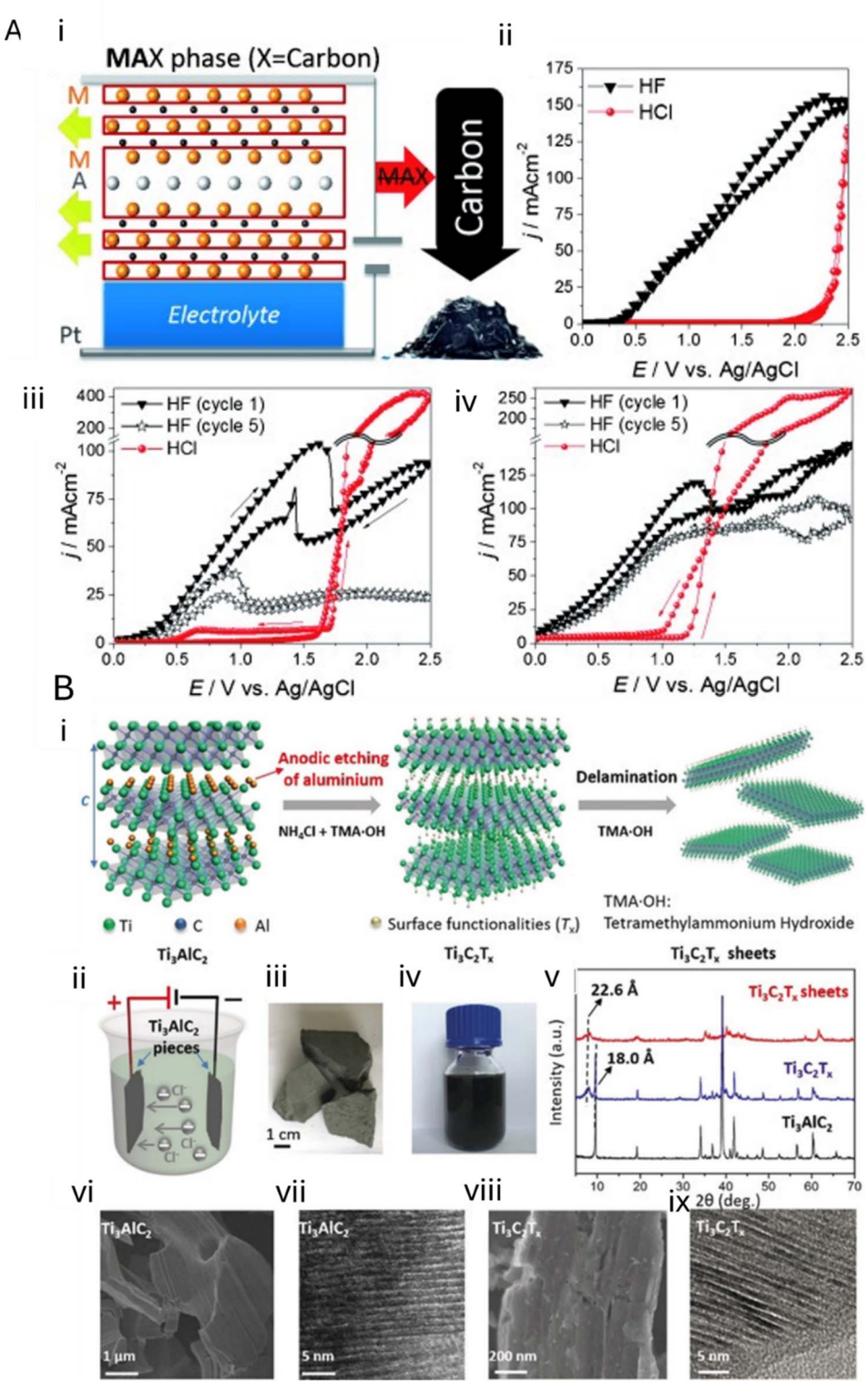

Fig. 7 (A) (i) Graphic demonstration of fabrication of the CDC from the MAX phase under room temperature conditions. Cyclic voltammograms acquired in HF (triangles) and HCl (circles) when (ii) Ti_3SiC_2, (iii) Ti_3AlC_2, and (iv) Ti_2AlC were employed as the anode. Reproduced with permission.[197] Copyright 2014, Wiley-VCH. (B) Anodic electrochemical etching of the bulk MAX phase Ti_3AlC_2 in the binary aqueous electrolyte solution. (i) Diagrammatic illustration of the electrochemical etching and the delamination procedure. (ii) The electrochemical system employed for the electrochemical etching. (iii) The acquired optical image of the as-received bulk MAX phase Ti_3AlC_2. (iv) Aqueous dispersion of the delaminated MXene $Ti_3C_2T_x$. (v) X-ray diffraction curves of different MAX phases – Ti_3AlC_2, MXene–$Ti_3C_2T_x$, and $Ti_3C_2T_x$ sheets. (vi and viii) SEM micrographs of the MAX phases Ti_3AlC_2 and $Ti_3C_2T_x$. (vii and ix) Cross-sectional HR-TEM micrographs of the MAX phase and MXenes Ti_3AlC_2 and $Ti_3C_2T_x$, respectively. Reproduced with permission.[199] Copyright 2018, Wiley-VCH.

Table 2 Electrochemical etching parameters of the MXene etching technique, electrolytic solution, voltage window, time duration, and temperature

MXene	Etching technique	Electrode setup	Electrolyte	Voltage	Time	Temperature	Ref.
Ti_2CT_x	Chronoamperometry	Three-electrode setup	1 M HCl	+0.6 V	1 day	[a]	198
Ti_2CT_x	Chronoamperometry	Three-electrode setup	2 M HCl	+0.6 V	5 days	[a]	198
$Ti_3C_2T_x$	Potentiometry	Two-electrode setup	1 M NH_4Cl + 0.2 M TMAOH	+5 V, actual +2.48 V (*vs.* SCE)	5 hours	[a]	199
Ti_2CT_x	Thermal assisted	Three-electrode setup	1 M HCl	0.3 V	9 hours	50 °C	200
V_2CT_x	Thermal assisted	Three-electrode setup	1 M HCl	0.5 V	9 hours	50 °C	200
Cr_2CT_x	Thermal assisted	Three-electrode setup	1 M HCl	1 V	9 hours	50 °C	200
$Ti_3C_2T_x$	—	—	1 M NH_4HF_2	2.5 V	2	[a]	201
$Ti_3C_2T_x$	—	—	1 M NH_4HF_2	5 V	2 hours	[a]	201
$Ti_3C_2T_x$	—	—	1 M NH_4HF_2	7.5 V	1.5 hours	[a]	201
$Ti_3C_2Cl_2$	Potentiometry	Three-electrode setup	LiCl–KCl	2.0 V	24 hours	[a]	172
Ti_2CT_x	Chronoamperometry	Three-electrode setup	LiCl and KCl	1.3 V *versus* ref	24 hours	500 °C	170
$Ti_3C_2T_x$	Chronoamperometry	Three-electrode electrochemical	[BMIM][PF_6]/MeCN	+3–+7 V *vs.* Ag wire	5 hours	[a]	202
$Ti_3C_2T_x$	—	Two-electrode system	0.8 M LiOH and 1.0 M LiCl	5.5 V	5 hours	[a]	203
$Ti_3C_2T_x$	Cyclic voltammetry scanning	Three-electrode setup	1 M NH_4Cl and 0.2 M TMAOH	−0.25 to 0.3 V	5 hours	[a]	204
Nb_2CT_x	—	Three-electrode setup	0.5 M HCl	1 V	4 hours	50 °C	205
V_2CT_x	Galvanic charge–discharge	Closed coin-type CR2030 cell	21 m LiTFSI + 1 m $Zn(OTf)_2$	400 cycles at 10 A g^{-1}	—	[a]	171
Mo_2TiC_2	—	Two-electrode system	0.93 M NH_4Cl and 0.42 M LiOH	5 V	2 hours	[a]	173
Mo_2TiC_2	—	—	Dilute HCl	0.7 V		55 °C	206
EE-Ti_3C_2	—	Two-electrode system	HBF_4	+1 V	28 hours	35 °C	145
EE-Ti_3CN	—	Two-electrode system	HBF_4	+1 V	28 hours	35 °C	145

[a] In the studies in which the temperature conditions were not mentioned, we considered that the reaction occurred under room temperature conditions.

Afterwards, the outer layer of Ti_2CT_x MXene, *i.e.*, $Ti_2C(OH)_{2x}$-Cl_yO_z, goes through additional electrochemical etching, where it is converted into the carbon-derived-carbon (CDC) layer with the functional groups like –O, –OH, and –Cl, owing to the concurrent elimination of both Al and Ti layers. Thus, when Ti is also eliminated, due to the over-etching procedure, it results in a core–shell structure, and TiO_2 is formed at the counter electrode (Pt), as shown in eqn (3). The proposed reaction mechanism of the electrochemical etching process is outlined as follows:

$$Ti^{4+} + 2H_2O \rightarrow TiO_2 + 4H^+ \quad (3)$$

Subsequently, Yang *et al.* reported another HF-free etching approach to electrochemically etch the MAX Ti_3AlC_2. This approach is based on the anodic corrosion of the MAX phase utilising a binary aqueous solution containing tetramethylammonium hydroxide (TMAOH) and ammonium chloride (NH_4Cl) as electrolytes.[199]

Following they performed physical and morphological characterisation to confirm the fabrication of MXene as illustrated in Fig. 7B. According to the experimental study, the following reaction mechanism is proposed:

$$Ti_3AlC_2 - 3e^- + 3Cl^- \rightarrow Ti_3C_2 + AlCl_3 \quad (4)$$

$$Ti_3C_2 + 2OH^- - 2e^- \rightarrow Ti_3C_2(OH)_2 \quad (5)$$

$$Ti_3C_2 + 2H_2O \rightarrow Ti_3C_2(OH)_2 + H_2 \quad (6)$$

where eqn (4) plays a crucial role in the eradication of aluminium metal from the MAX phase anode. Next, the –OH terminal group is introduced on the MXene surface, as illustrated in eqn (5) and (6). Furthermore, the intercalation of ammonium ions and the removal of the Al metal are taking place concurrently. The following reaction mechanisms are proposed in eqn (7) and (8). This HF-free electrochemical etching results in the formation of mono- and bilayers of MXenes ($Ti_3C_2T_x$, T–OH, and –O) with a high yield of up to 90% and sizes of up to 18.6 μm. The obtained MXene exhibited a volumetric capacitance of 439 F cm^{-3} and an areal capacitance of 220 mF cm^{-2} with a scan rate of 10 mV s^{-1} for all solid-state supercapacitor applications.[199] The synthesis of MXene *via* the electrochemical etching approach opens avenues for more sustainable and eco-friendly ways to fabricate different varieties of MXenes with different terminal groups, resulting in enhanced electrochemical performance.

$$AlCl_3 + 3NH_3 + 2H_2O \leftrightarrow AlO(OH) + 3NH_4^+ + 3Cl^- \quad (7)$$

$$AlCl_3 + 2OH^- \leftrightarrow AlO\,(OH) + H^+ + 3Cl^- \quad (8)$$

3. Electrochemical etching of Ti-based MXenes

The thermal electrochemical etching route was reported by Pang *et al.* for the synthesis of Ti-based MXenes, and they extended this method to other transition metal-based MXenes like Cr and V, calling it a universal method, using a three-electrode system employing HCl as the electrolyte by varying the temperature, time, and voltage parameters. The SEM images are provided to confirm the successful etching of MAX to MXene, varying different parameters (Fig. 8A). In this approach, different MAX phases, such as Cr_2AlC, Ti_2AlC, and V_2AlC, are mixed separately with carbon black to fabricate the corresponding 3D composite MXene electrodes.[200] These electrochemically etched MXene electrodes doped with the cobalt ions demonstrate a superior capability for catalysing multiple electrochemical reactions, including the HER, OER, and zinc ion batteries. In addition, Cao *et al.* fabricated electrochemically etched MXene (Ti_3C_2) with –O/–OH and –F terminal groups under room temperature conditions using 1 M NH_4HF_2 aqueous solution. They provided the following etching parameters, varying voltage and time as follows: 2.5 V for 2 h, 5 V for 2 h, and 7.5 V for 1.5 h, demonstrating that synthesised MXene has a larger surface area and a narrow pore size distribution[201]

Another major challenge in MXene fabrication is to fabricate MXene with different terminal groups. To resolve this issue, the molten salt assisted electrochemical etching approach for fabrication of a –Cl terminated MXene ($Ti_3C_2Cl_2$) was reported by Shen *et al.* In this approach, the terminal groups of MXene are *in situ* modified from –Cl to –S and/or –O using different inorganic salts, which leads to the shortening of the modification stages and additionally increases the different types of terminal groups in MXenes (Fig. 8B). In this approach, Ti_3AlC_2 acts as the anode and nickel acts as the cathode in the LiCl–KCl salt, and a voltage of 2.0 V is applied at 450 °C. However, the real operational bias on the anode attained 0.365 (V *vs.* Ag/AgCl). At this stage, the Al metal atoms from the MAX phase are selectively oxidised and eliminated owing to the weaker Ti–Al bonds in comparison to the Ti–C bonds. Subsequently, the oxidised Al forms a bond with the Cl ions present in the electrolytic solution, forming $AlCl_3$ because of their robust binding capabilities.

Additionally, at 450 °C, the evaporation of $AlCl_3$ occurs, initiating the driving force for the diffusion of Al outwards. As this etching process is thermodynamically influenced, the applied potential plays a significant role.[172] The acquired O-terminated MXene is an outstanding electrode for energy storage applications (supercapacitor), demonstrating a capacitance of 225 F g^{-1} at a current density of 1.0 A g^{-1} with a rate performance of 91.1% at 10 A g^{-1} and an outstanding capacitance retention of 100%. This synthesis process is considered more sustainable because no acid waste is generated, and the salt can be recycled. The reaction mechanisms for electrochemical etching are depicted below (eqn (9)–(12)):

Anode:

$$Ti_3AlC_2 + 3Cl^- = AlCl_3\uparrow + Ti_3C_2 + 3e^- \quad (9)$$

$$Ti_3C_2 + 2Cl^- = Ti_3C_2Cl_2 + 2e^- \quad (10)$$

Cathode:

$$Li^+(K)^+ + e^- = Li(K) \quad (11)$$

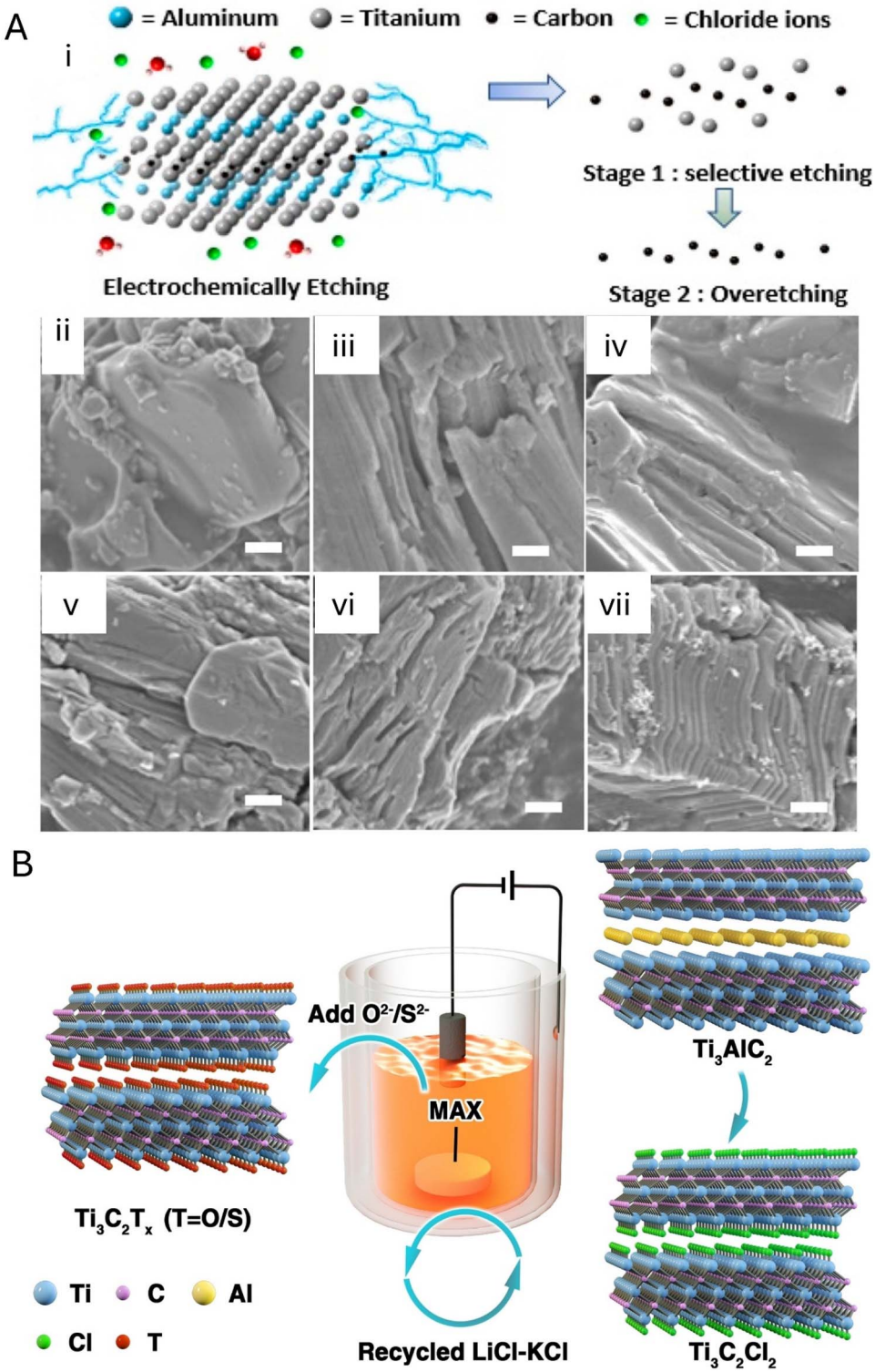

Fig. 8 (A) Electrochemical etching reaction mechanism and structural conclusions of the MXene Ti_2CT_x. (i) Anticipated electrochemical etching reaction mechanism route of the MAX phase Ti_2AlC in the HCl electrolyte solution. SEM micrographs of the MXene were obtained under varying HCl, temperature, time and voltage electrochemical etching conditions. (ii) MAX Ti_2AlC, (iii) 1 M/25 °C/9 h/0.3 V, (iv) 1 M/50 °C/3 h/0.3 V without CB, (v) 1 M/50 °C/3 h/0.3 V, (vi) 1 M/50 °C/6 h/0.3 V, and (vii) 1 M/50 °C/9 h/0.3 V. Scale bars: 1 μm. Reproduced with permission.[200] Copyright 2019, American Chemical Society. (B) Illustration of the fabrication process of MXene from the corresponding MAX phase through MS-electrochemical etching, followed by the *in situ* modification of surface terminations. Reproduced with permission.[172] Copyright 2021, Wiley-VCH.

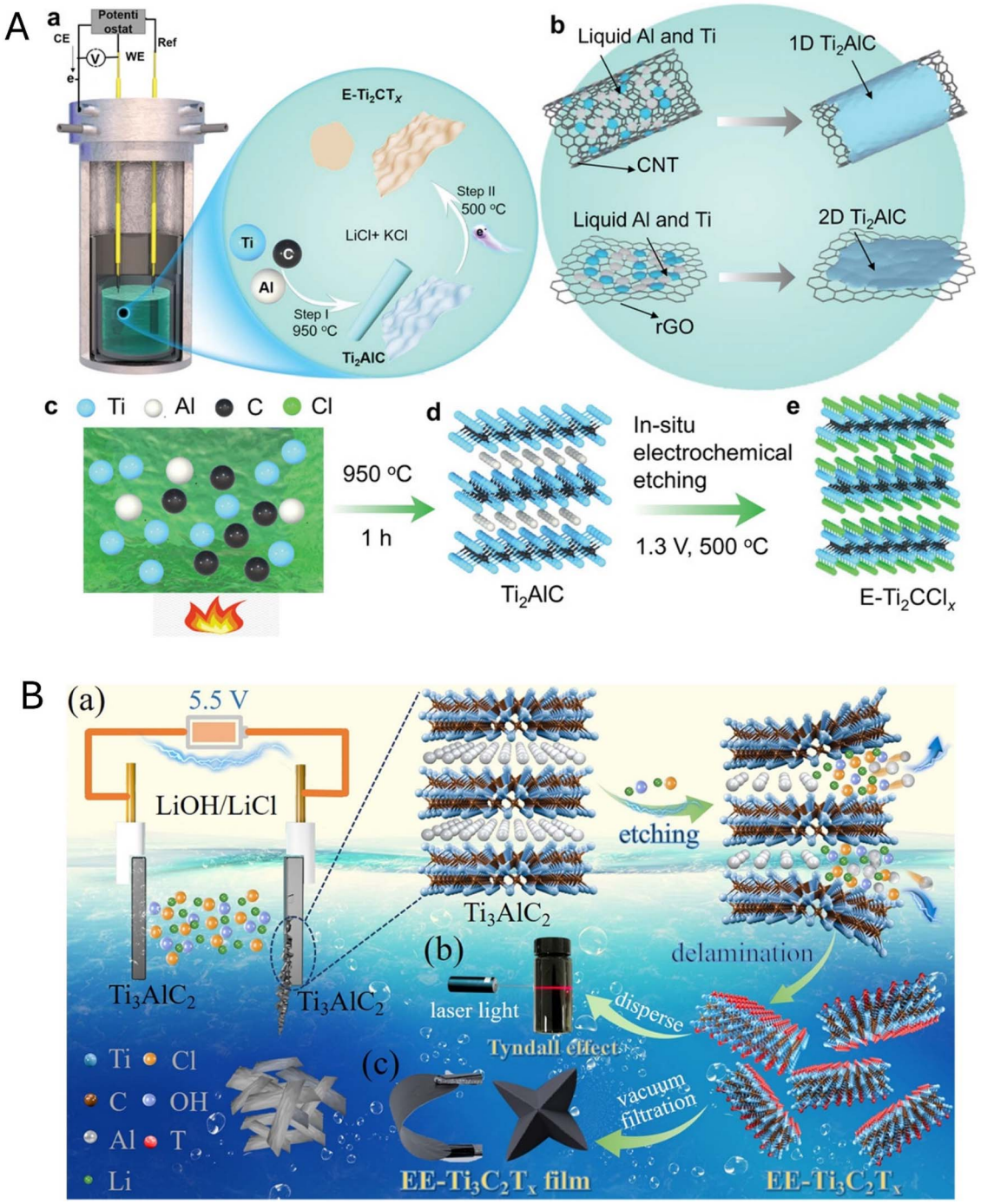

Fig. 9 (A) Graphic visual of the production process of the MAX phase Ti_2AlC and MXene E-Ti_2CT_x. (a) The graphic illustration of the setup employed for the electrochemical etching. (b) The diagrammatic representation of the production of 1D and 2D Ti_2AlC structures employing CNTs and rGO as their carbon resources. (c) The Ti, Al, and C pellets were immersed in LiCl/KCl, followed by heating at 950 °C for 1 hour. (d) The fabrication of the MAX phase Ti_2AlC. (e) Following the electrochemical etching process at a voltage of 1.3 V for 24 hours to achieve the E-Ti_2CCl_x MXene. Reproduced with permission[170] Copyright 2022, Wiley-VCH, under Creative Commons Attribution-NonCommercial License.[78] (B) (a) Diagrammatic representation of the production of MXene EE-$Ti_3C_2T_x$. (b) Images of MXene dispersion illustrating the Tyndall effect. (c) Images of the MXene films. Reproduced with permission.[203] Copyright 2022, American Chemical Society.

Overall:

$$Ti_3AlC_2 + 5LiCl(KCl) = Ti_3C_2Cl_2 + 5Li(K) + AlCl_3\uparrow \quad (12)$$

Subsequently, Liu *et al.* reported a one-pot molten salt electrochemical etching approach. A straightforward technique is to synthesise chlorine-terminated MXene (Ti_2CCl_x) from its precursor elements (Ti, Al, and C). This method significantly simplifies the MXene synthesis procedure, where Ti and Al micro-powders are reacted with the carbon nanotubes (CNTs) and reduced graphene oxide (rGO), which serve as different

carbon sources. To fabricate the MAX (Ti_2AlC) phase with tunable morphologies like 1D and 2D structures (Fig. 9A), concurrently, the MAX phase is converted into MXene utilising an electrochemically etching method in a cost-effective LiCl–KCl solution. The pseudocapacitive redox reaction of MXene can be initiated with the introduction of an –O surface terminal group and ammonium persulfate washing (APS), which can lead to a better Li^+ storage capacity of approximately up to 857 C g^{-1} (240 mAh g^{-1}) with a high rate capability of 86 mAh g^{-1} at 120C, thus generating promising anode materials for fast-charging batteries for energy storage applications.[170]

The fabrication of MXenes with controlled fluorine termination is another concern. In this context, Yin *et al.* introduced synchronous fluorination and mild-electrochemical exfoliation of $Ti_3C_2F_x$ MXene using RTIL [BMIM][PF_6] as the –F source and MeCN. This ionic liquid electrolyte offers a non-aqueous etching environment to prevent MXene oxidation. The fabricated MXene was fluorinated utilising TiF_3 and CF groups. These groups were electrochemically reactive, and they contributed to the electrochemical performance of the fabricated $Ti_3C_2F_x$. This fluorinated $Ti_3C_2F_x$ anode exhibited excellent cycling stability for lithium-ion battery applications, demonstrating a charge capacity of 329 mAh g^{-1} (initially) at the current density of 200 mA g^{-1}. Following 500 cycles, the charge capacity of 211 mAh g^{-1} was maintained. Moreover, in this study, they demonstrated that the fluorination of $Ti_3C_2F_x$ can be regulated through adjusting the fabrication conditions.[202]

The use of hazardous organic intercalant agents for the delamination of MXene is a major issue. To resolve this issue, Chen *et al.* reported a simplified route to fabricate Ti_3C_2 MXene, without using any organic intercalant agent for delamination. In this study, they reported electrochemical etching of the MAX phase utilising a mixture of LiOH and LiCl aqueous solution to produce chlorine-terminated MXene, and later sonication was used to delaminate the obtained MXene (Fig. 9B). The acquired delaminated chlorine-terminated MXene flake sizes range from ~3.9 nm to ~3.8 μm in thickness and lateral size, respectively, with the stability of up to 15 days, when dispersed in an aqueous solution.[203] Following that, a vacuum filtration technique was utilised to fabricate MXene films. The obtained filtrate MXene films were used for electrochemical energy storage applications, *i.e.*, supercapacitors and exhibited excellent capacitances of 323.7 F g^{-1}, 1.39 F cm^{-2}, and 1160 F cm^{-3}, respectively, outperforming the conventionally fabricated MXene. According to the experimental results, the following equations are proposed to illustrate the etching mechanism (eqn (13)–(15)):

$$Ti_3AlC_2 + 3Cl^- + 3e^- \rightarrow Ti_3C_2 + AlCl_3 \quad (13)$$

$$Ti_3C_2 + xCl^- + (2-x)OH^- - 2e^- \rightarrow Ti_3C_2Cl_x(OH)_{2-x} \quad (14)$$

$$AlCl_3 + 2OH^- \rightarrow AlOOH + H^+ + 3Cl^- \quad (15)$$

Additionally, the fluoride (–F) terminal group of MXene drastically impacts the charge transfer efficiency and hinders ion access to MXene (Ti_3C_2). To overcome this obstacle, Qian *et al.* introduced fluoride termination-free $Ti_3C_2T_x$ MXene fabrication. In this study, to electrochemically etch the MAX phase, a three-electrode setup was used employing the cyclic voltammetry technique using 1 M NH_4Cl and 0.2 M TMAOH as the electrolyte.[204] An exact potential range of −0.25 to 0.35 V was applied at room temperature for 5 hours with constant stirring of 300 rpm. During this process, an *in situ* alkaline electrolyte was formed, destroying the Ti–Al bonds and aiding in the formation of –AlO(OH) and –OH terminal groups on the surface of $Ti_3C_2T_x$ MXene (Fig. 10a and b). The SEM images, along with the EDS mapping and XRD pattern, confirm the successful

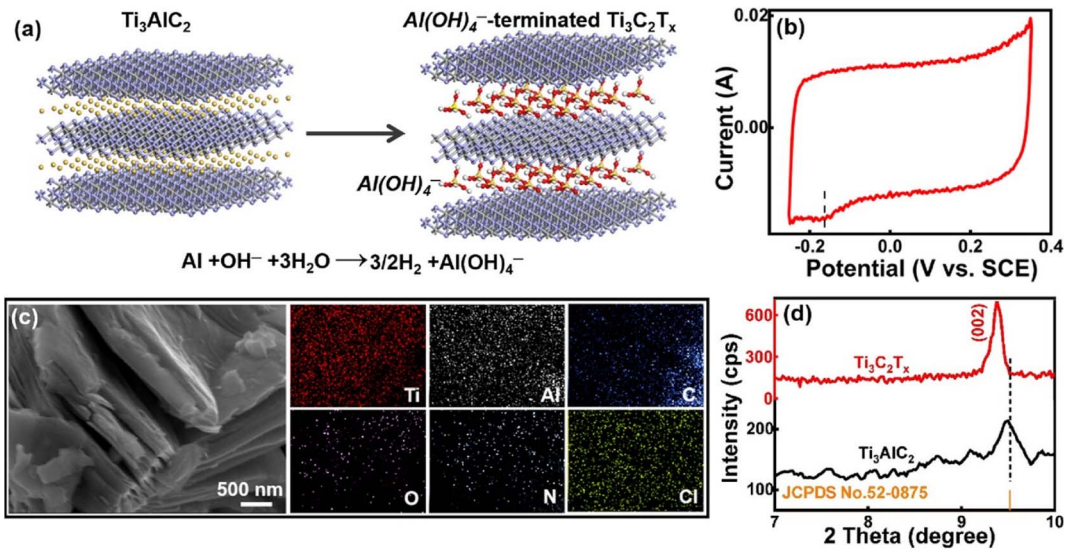

Fig. 10 (a) Schematic illustration of the fabrication process and morphological structure of the fluoride-free electrochemical etched MXene $Ti_3C_2T_x$. (b) The three-electrode configuration was employed to acquire the CV scan for the MAX electrode with a scan rate of 20 mV s^{-1}, (c) SEM and elemental mapping analysis images, and (d) XRD patterns of MXene and MAX phase. Reproduced with permission.[204] Copyright 2023, American Chemical Society.

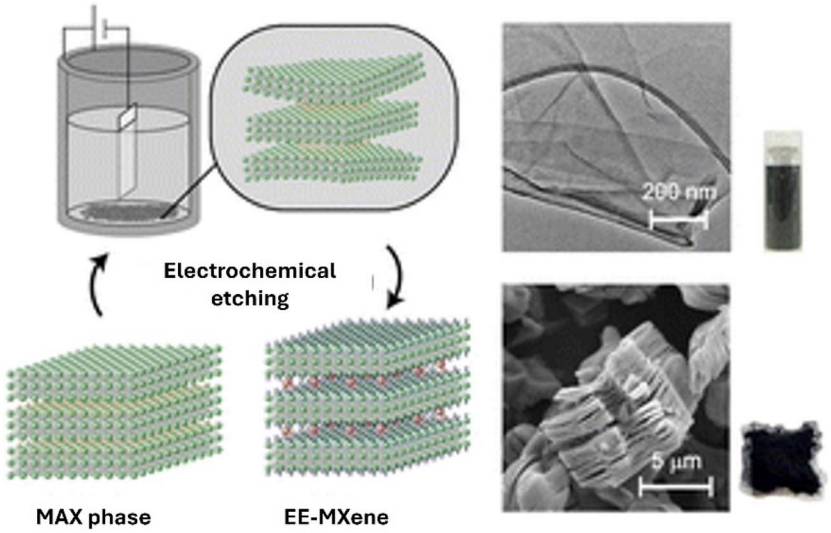

Fig. 11 Schematic illustration of the low-fluoride electrochemical etching fabrication of MXene along with the TEM micrograph of delaminated MXene and SEM micrographs of MXene powder. Reproduced with permission.[145] Copyright 2024, The Royal Society of Chemistry under Creative Commons Attribution 3.0 Unported License.

fabrication of MXene (Fig. 10c and d). The fabricated MXene was employed for capacitive deionisation (CDI) device application delivering an outstanding salt elimination capacity of 20.27 mg^{-1} with an adsorption rate of 1.01 mg g^{-1} min^{-1} because of the improved ion transport capability and hydrophilicity of etched $Ti_3C_2T_x$.

Additionally, Chan *et al.* reported low fluoride electrochemical etching of two titanium-based MAX phases, Ti_3AlC_2 and Ti_3AlCN, to formulate the corresponding MXene Ti_3C_2 and Ti_3CN employing HBF_4 as the electrolyte solution. The electrochemical etching process occurs in a graphite crucible, where it also acts as the current collector to the MAX phase powder and a platinum (Pt) wire serves as the cathode electrode.[145] In this electrochemical etching procedure, no binder is required as the etching of the MAX phases Ti_3AlC_2 and Ti_3AlCN is possible in its powder state, as all the MAX particles are settled down on the graphite crucible at the time of the electrochemical etching procedure (Fig. 11). The reaction mechanism is proposed as follows for this electrochemical etching route (eqn (16)–(18)):

Anode:

$$Ti_3AlC_2(s) + 3BF_4^-(aq.) \rightarrow Ti_3C_2(s) + Al^{3+}(aq.) + 3F^-(aq.) + BF_3(g) + e^- \quad (16)$$

Cathode:

$$H^+(aq.) + e^- \rightarrow 1/2H_2(g) \quad (17)$$

Overall:

$$Ti_3AlC_2(s) + 3HBF_4(aq.) \rightarrow Ti_3C_2(s) + 3BF_3(g) + AlF_3(s) + 3/2H_2(g) \quad (18)$$

According to the reaction mechanism, during the electrochemical etching process, the selective anodic dissolution of the aluminium metal occurs on the MAX phase Ti_3AlC_2 with the tetrafluoroborate ion. This electrochemical etching pathway reduces the etching time. Thus, the release of the HF gas is minimal. Furthermore, the electrochemically etched MXenes are tested for the energy storage application for lithium-ion batteries and demonstrate similar electrochemical performance compared to the chemically etched MXene. Following that, Zheng *et al.* reported electrochemical synthesis of TiC and carbon-derived carbon using Ti_3SiC_2 in $CaCl_2$ molten salt at 900 °C with potentials 2.5 V and 3.0 V, respectively, illustrating that non-Al precursors can be employed to fabricate MXene using an electrochemical etching strategy.[207]

Besides, novel techniques can be explored to synthesise MXene *via* electrochemical etching; for example, based on our previous work, we formulated a 3D-printed MAX/PLA electrode and investigated its *in situ* electrochemical etching process to convert into an electrochemically active 3DP-etched MAX electrode. In this process, the electrodes were washed with distilled water and used directly for electrochemical analysis, without any separation from the polymer, which exhibits promising electrochemical performance, highlighting the capability of direct use of these electrodes for various applications, unlike the traditional carbon-based electrodes, which require additional formulation steps and lack precision. However, several challenges persist in obtaining large quantities of pure MXene, as separation from polymer is a challenging process.[37]

4. Electrochemical etching of Nb, V, Mo-based MXene

The most extensively studied MAX phase until now is the titanium transition metal-based MAX phase. Thus, exploration of other MAX phases and their corresponding MXenes is becoming more prominent. In this context, Song *et al.* reported

an electrochemical etching technique to fabricate Nb_2CT_x MXene using the Nb_2AlC MAX phase as the precursor. The electrochemical etching was performed in a three-electrode setup utilising 0.5 M HCl as the electrolyte by providing a voltage of under 1 V for 4 hours.[205] The aluminium metal was selectively etched *via* anodization at a temperature of 50 °C. The electrochemical etching reaction mechanism for Nb_2AlC is proposed in eqn (19):

$$Nb_2AlC + yCl^- + (2x + z)H_2O \rightarrow Nb_2C(OH)_{2x}Cl_yO_z + Al^{3+} + (x + z)H_2\uparrow + (y + 3)e^- \quad (19)$$

The synthesised electrochemically etched MXenes were purified. The fluoride-free Nb_2CT_x–acetylcholinesterase (AChE)-based electrochemical biosensors were assembled for phosmet detection. These fabricated materials provide a limit of detection of as low as 0.046 ng mL^{-1}. This fluoride-free electrochemically etched MXenes have advantages such as improved electron transfer potential and better enzyme activity compared to the traditional HF-based etched MXenes (Fig. 12A).

Additionally, Sheng *et al.* recently reported a sustainable approach using two-electrode configurations to fabricate 3D MXene electrodes from the precursor Mo_2TiAlC_2 MAX phase[173]

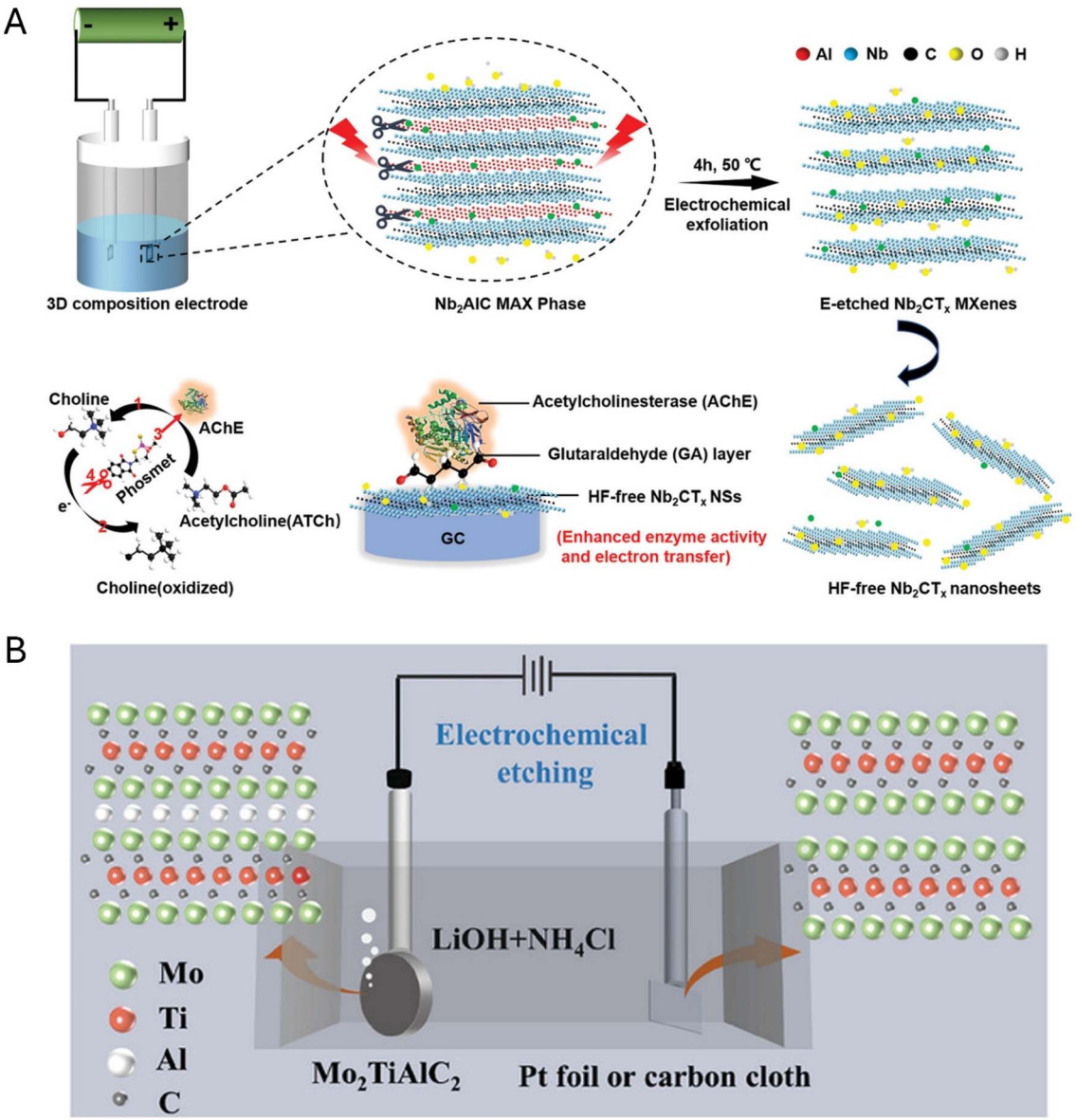

Fig. 12 (A) Graphic illustration of the electrochemical exfoliation and delamination routes for the MAX phase (Nb_2AlC) through the electrochemical etching method, followed by demonstrating the enzyme inhibition effect for phosmet detection employing an electrochemically etched MXene Nb_2CT_x/AChE biosensor. Reproduced with permission.[205] Copyright 2020, Wiley-VCH under CC-BY License. (B) A graphic visual for the electrochemical etching procedure of Mo_2TiC_2 MXene fabrication from their corresponding MAX phase. The two-electrode configuration is employed, where Pt foil or carbon cloth acts as the cathode electrode and Mo_2TiAlC_2 MAX phase block acts as the anode electrode, followed by using an NH_4Cl and LiOH mixture as the electrolyte. Reproduced with permission.[173] Copyright 2023, Wiley-VCH.

(Fig. 12B). They employed a synergistic blend of cathodic electrophoretic deposition and anodic electrochemical etching of the Al layer from the corresponding MAX phase. This process is less time-consuming compared to the conventional MXene fabrication process, as the MXene (Mo_2TiC_2) was obtained without the use of an ultrasound and large organic molecule intercalation reagent treatment. Within few minutes, MXene (Mo_2TiC_2) was deposited onto the cathode part (carbon cloth or platinum). Additionally, this route is beneficial as less acid waste is generated compared to the traditional MXene fabrication process. Because it allows an effective way to separate the fabricated MXene (Mo_2TiC_2) from the electrolytic solution, as it is directly uniformly deposited onto the cathode part. This electrochemically etched Mo_2TiC_2 deposited on the carbon cloth surface can be directly employed as a 3D MXene electrode electrocatalyst material for energy conversion applications like the HER.

The conventional multistep process of synthesis of MXene from MAX using toxic chemical reagents, followed by device fabrication, is time-consuming. Thus, to tackle this issue, Li *et al.* introduced a straightforward method by employing the V_2AlC MAX phase as the cathode, Zn metal as the anode and 21 M LiTFSI + 1 M Zn $(OTf)_2$ as the electrolyte solution, for the fabrication of a closed coin-type CR2030 device for battery testing application.[171] Because of the selection of F-enriched solution as the electrolyte, it promotes the exfoliation of the V_2AlC MAX phase, resulting in the formation of V_2CT_X MXene inside the battery cell directly, as confirmed by the morphological characterisation of the MXene cathode after the electrochemical performance of about 400 cycles at 10 A g^{-1}, as illustrated in the SEM image in Fig. 13a. It is demonstrated that the microstructure of the MXene cathode alters significantly, where the V_2AlC MAX phase particles are converted into V_2CT_X MXene, which is evident in the magnified SEM image in Fig. 13b.

This conversion of V_2AlC MAX to V_2CT_X MXene is similar to the conventional wet chemistry etching process, with the smoother outer surface of V_2CT_X MXene without any impurities,

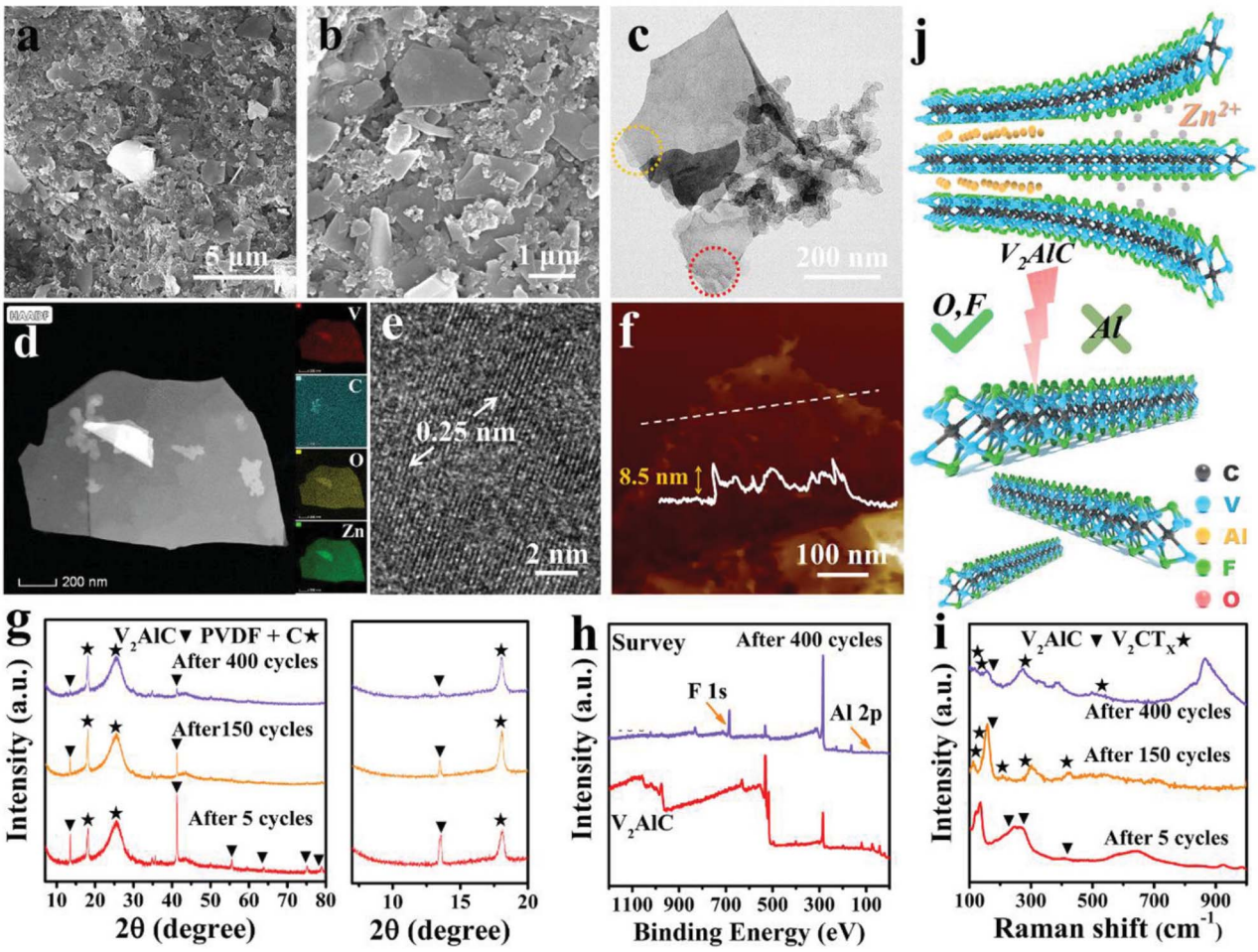

Fig. 13 Physical and morphological characterisation of the *in situ* produced MXene V_2CT_X and their reaction mechanism. (a and b) SEM micrographs of the cathode, (c) transmission electron microscopy (TEM) micrograph. (d) TEM micrograph in the HADDF mode for EDS mapping analysis; insets display the V, C, O, and Zn elements related to MXene. (e) High-resolution TEM micrograph. (f) AFM micrograph. (g) XRD patterns at different cycles. (h) Wide survey XPS spectra. (i) Raman spectra at different cycles. (j) Graphic demonstration of the *in situ* electrochemical etching process reaction mechanism. Reproduced with permission.[171] Copyright 2020, Wiley-VCH.

Table 3 The electrochemical etching of MXene, including the technique, etching agent, terminal groups, advantages and applications

MXene	Technique	Etching agent	Terminal group	Advantage	Application	Ref
Ti_2CT_x	Electrochemical etching	HCl	–OH, –O, and –Cl	Dilute HCl solution	—	198
$Ti_3C_2T_x$	Electrochemical etching	NH_4Cl + TMAOH	–OH and –O	High yield (over 90%) mono- and bilayers	Solid-state supercapacitor	199
Ti_2CT_x, Cr_2CT_x, and V_2CT_x	Electrochemical etching	HCl	–OH, –O, and –Cl	Universal strategy	Hydrogen evolution reaction (HER), oxygen evolution reaction (OER) and rechargeable battery	200
$Ti_3C_2T_x$	Electrochemical etching	NH_4HF_2	–F and –O/–OH	Room temperature	—	201
$Ti_3C_2T_x$	Molten-salt-assisted electrochemical etching		–Cl to –O and/or –S	The surface terminations can be *in situ* modified	Supercapacitor	172
Ti_2C	Electrochemical etching	LiCl/KCl	–Cl and –O	1D and 2D tuned morphology	Li-ion storage	170
$Ti_3C_2T_x$	Electrochemical etching	$[BMIM][PF_6]$/MeCN	–F and –O/–OH	Controllable fluorination	Lithium-ion batteries	202
$Ti_3C_2T_x$	Electrochemical etching	LiOH and LiCl	–Cl	Delamination *via* sonication	Supercapacitor/zinc ion hybrid capacitor	203
$Ti_3C_2T_x$	Electrochemical etching	NH_4Cl + TMAOH	–AlO(OH)– and –OH–	High salt-removal capacity	Capacitive deionisation (CDI)	204
Nb_2CT_x	Electrochemical etching	HCl	—	Chemical stability and biocompatibility	Electrochemical biosensors	205
V_2CT_X	Electrochemical etching	$C_2F_6LiNO_4S_2$ salt (LiTFSI) and $Zn(CF_3SO_3)_2$ salt ($Zn(OTf)_2$)	–F	All-in-one protocol	Zinc-ion battery	171
Mo_2TiC_2	Electrochemical etching	LiOH/NH_4Cl	–OH, –O, and –Cl	Deposition on the cathode plate	Hydrogen evolution reaction	173
$MoTi_2C$	Electrochemical etching	HCl	–OH, –O, and –Cl	The active site to capture S ions	Hydrogen evolution reaction	206
Ti_3C_2 and Ti_3CN	Electrochemical etching	Tetrafluoroboric acid	—	Larger lateral dimension of MXene	Lithium-ion supercapacitors	145

and the lateral size of V_2CT_X MXene ranges between 1 and 5 μm. The A layers are removed along with the –O, –F and –OH terminals formed in a parallel direction to (001), which results in the preservation of original lamellar structures. The TEM images illustrated in Fig. 13c show classic electron beam transparent characteristics. Additionally, the etching of aluminium layers was confirmed utilising EDS mapping with the Al content less than 0.37 atomic%, as shown in Fig. 13d. Furthermore, the high-resolution transmission electron microscopy analysis (HR-TEM) shows the ordered lattice fringe in Fig. 13e, further confirming the high crystallisation of the *in situ* electrochemical etched V_2CT_X MXene.

Additionally, the atomic force microscopy (AFM) images illustrated in Fig. 13f show that the thickness of the V_2CT_X MXene is concentrated at 8.5 nm, suggesting that the number of layers is five or seven. The X-ray diffraction further proves the phase transition from V_2AlC MAX to V_2CT_X MXene, as the XRD pattern is obtained after 5, 150, and 400 cycles. At 5 cycles, the V_2AlC MAX phase and additive (polyvinylidene, carbon cloth and carbon black) diffraction peaks are presently displayed in Fig. 13g. Nonetheless, after increasing the number of cycles, *i.e.*, at 150 cycles, the peaks of the V_2AlC MAX phase are diminishing, suggesting the conversion from V_2AlC MAX to V_2CT_X MXene. Following 400 cycles, the V_2AlC MAX phase peak is barely visible, specifically in the peak regions of 13.3° and 41.3°, which are associated with the (002) and (103) crystal planes. It can be suggested that after 400 cycles, the V_2AlC MAX phase is successfully exfoliated. To better understand the etching of Al metal, the survey X-ray photoelectron spectroscopy (XPS) spectra were obtained, as displayed in Fig. 13h, which validated the XRD results, confirming the eradication of Al metal at 73 eV and the addition of a new peak at 685 eV after 400 cycles. This conversion of V_2AlC MAX to V_2CT_X MXene was further validated by Raman spectra, as illustrated in Fig. 13g. The Raman peaks associated with the V_2AlC MAX phase at 158, 239, and 258 cm^{-1} were diminishing. While the Raman peaks at 114, 139, 262, and 298 cm^{-1} corresponding to V_2CT_X MXene were dominating. The following reaction mechanism was proposed, based on the observations (eqn (20)).

$$V_2AlC + yF^{-1} + (2x + z)H_2O - (y + 3)e^{-1} \rightarrow V_2C(OH)_{2x}F204_yO_z + Al^{3+}(Al_2O_3, AlF_3) \quad (20)$$

So, Fig. 13j displays the breaking of the V–Al bonds in the V_2AlC MAX phase cathode as it was attacked by F^{-1}, which is present in the electrolytic solution, resulting in the etching of Al layers and forming V_2CT_X MXene. In the single-step procedure, the battery device undergoes three phases: MAX exfoliation, electrode oxidation and redox of V_2O_5. This device can be directly used for battery testing applications while all the reactions are undergoing, and it is observed that the electrochemical performance keeps increasing. Moreover, this battery device exhibited excellent electrochemical performance for a zinc ion battery, demonstrating cycling stability of 4000 cycles with the rate performance of 97.5 mAh g^{-1} at 64 A g^{-1}. According to this study, this *in situ* electrochemically etched MXene with its high capacity outperform the other reported vanadium-based zinc ion batteries.

This single-step, straightforward green fabrication process of MXene, followed by device assembly, prevents any contamination from outside and expands the applications of MXene in the field of aqueous energy storage devices. Overall, the electrochemical etching strategies hold particular importance in the realm of MXenes, contributing towards a harmless and more precisely controlled approach to synthesize MXene. These strategies have garnered significant attention due to their ability to avoid the dangers related to the fluorine compounds while producing MXene with tunable properties. A summary of electrochemical etching of MXene, including the technique, etching agent, terminal groups, advantages and their applications, is provided in Table 3.

5. Conclusion, challenges, and future outlooks

This review article emphasises the comprehensive study of the electrochemical etching route for the fabrication of MXenes, centering on its fundamental mechanism and the different parameters that impact the electrochemical etching of the aluminium layer from the MAX phase to fabricate the corresponding MXene. The electrochemical etching synthesis of MXene has attracted significant research attention as a substitute for the conventional HF-based etching route, owing to its capability to produce MXene with varying terminal groups like –O, –OH, and –Cl.

Additionally, several benefits of electrochemical etching fabrication processes are highlighted, such as this approach being green, sustainable, less waste-generating, and cost-effective, without using any tedious process. Moreover, emphasis is given to the exploration of MXenes derived from other than titanium-based MAX phases, as to date, most reported studies are on titanium-based MXenes fabricated through electrochemical etching. This review article focuses on the electrochemical etching fabrication process of MXenes like Nb_2CT_x, V_2CT_X, and Mo_2TiC_2 and their outstanding performance for multiple applications in diverse fields, from biomedical to energy storage and conversion, highlighting their huge potential for the future.

Despite the ongoing research in the production of electrochemically etched MXenes, it exhibits various obstacles that need to be resolved for efficient production and real-world applications. The fundamental issues lie in the tuning of the etching parameters, including the selection of a suitable electrolyte solution, duration of etching and voltage window, to attain a uniformly delaminated MXene, concurrently preventing the over-etching of the MXene and maintaining its structural integrity. Because the inappropriate etching parameters can cause defects in MXene, reduced electrical conductivity, stability and residual aluminium impurities, which severely impede its electrochemical performance. One of the most crucial parameters to decide the properties of obtained MXenes, their oxidation resistance and intercalation capability, is

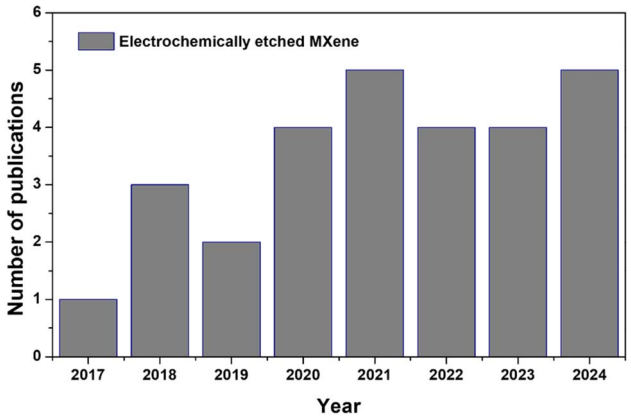

Fig. 14 The number of publications on electrochemically etched MXenes *vs.* years (search performed on Google Scholar using the keywords 'electrochemical etching of MXene').

through the optimisation of the electrolytic solution. Thus, the selection of the proper electrolytic solution is a crucial parameter.

Another major challenge is mass-scale production, while electrochemical etching provides a sustainable and safer route to fabricate MXene compared to chemical etching. But retaining the consistency when the production is large-scale is still challenging. Moreover, several obstacles, including oxidation of MXene and long-term stability after the electrochemical etching, need to be resolved, as the MXene oxidation leads to a compromise in the electrical and mechanical properties of MXene, resulting in poor electrochemical performance in various electrochemical applications, from energy storage to conversion and biomedical fields. These issues can be resolved by addressing the appropriate selection of electrolytes and the post-etching process to ensure the manufacturing of high-quality MXene for the advancement of MXene's future research. The electrochemical etching strategy has been garnering significant attention since its discovery, as evidenced by the increase in the number of publications each year (Fig. 14).

The future direction of the electrochemical etching route to fabricate MXene lies in the evolution of the current technologies. To enhance the MXene fabrication efficiency, through optimisation of the MXene properties and terminal groups designed for specific applications, exploration of novel electrolytes, scalability, stability, integration of modern technology with more eco-friendly routes (Fig. 15).

(1) The MXene fabrication efficiency could be enhanced through the modification of MXene's electrical and mechanical properties, by modulating the electrochemical etching parameters to attain precise control over the MXene structure, selective etching of the A layer and integrating the specific terminal groups for specific applications to boost the MXene electrochemical competence.

(2) Real-time monitoring methods like *in situ* spectroscopy and theoretical studies like density functional theory (DFT) may be beneficial to better understand the electrochemical etching route at a molecular scale, letting the researchers modulate the electrochemical etching conditions for enhanced consistency and high-quality MXene.

(3) Exploring novel electrolyte solutions like green solvents and neutral electrolytes for electrochemical etching of selective A-layers that are efficient, less toxic and sustainable could be a promising approach to fabricate electrochemically etched MXene. Most of the conventional approaches are dependent on corrosive acidic electrolytes, which pose safety threats.

(4) The mass-scale economic production of MXene for industrial applications should be the focus of the scientific community. To design and innovate the electrochemical etching routes with advanced features, to avail the MXenes

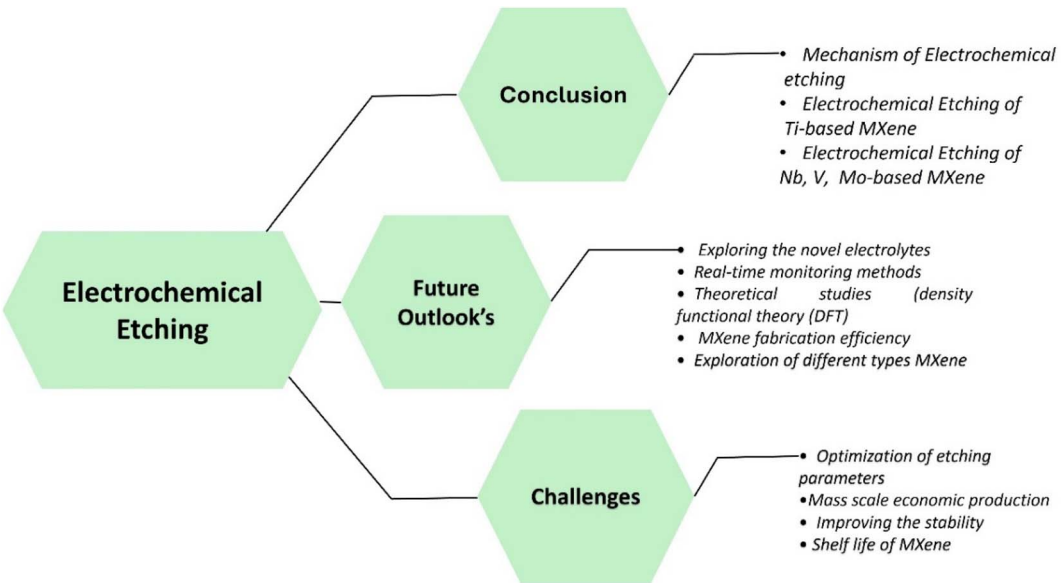

Fig. 15 The outline of the review article.

commercially, high-throughput production methods like roll-to-roll manufacturing and large-batch fabrication must be explored.

(5) Improving the stability of the electrochemically fabricated MXene is another potential direction for future studies for its long-term practical applications as degradation and oxidation of MXene severely impede its electrochemical activity.

(6) Integrating different strategies to fabricate different types of MXene composite with other 2D materials like Prussian blue frameworks, COFs, MOFs, and HOF materials[208–212] could be explored in future. Additionally, proper storage conditions and stability of fabricated MXene needs to be improved, which can lead to enhanced electrochemical performance. Thus, resulting MXene could be more appropriate for various purposes like sensing, catalysis, bio-medical, electrochemical energy conversion and storage applications. With the current progress in this area of MXene fabrication, electrochemical etching is projected to become one of the leading techniques for MXene production, encouraging their extensive employment in next-generation expertise.

Conflicts of interest

The authors of the review article possess no conflict of interest.

Data availability

Data will be available at the public repository ZENODO.

Acknowledgements

The present review article was sponsored by ERDF/ESF TECHSCALE (No. CZ.02.01.01/00/22_008/0004587) and co-sponsored by the European Union in REFRESH – Research Excellence For REgion Sustainability/High-tech Industries (project number CZ.10.03.01/00/22_003/0000048) by Operational Programme Just Transition. M. P. acknowledges project ANGSTROM for funding. Project ANGSTROM was selected in the Joint Transnational Call 2023 of M-ERA.NET 3, which is an EU-funded network of about 49 funding organisations (Horizon 2020 grant agreement No 958174). This project "Advancing Supercapacitors with Plasma-designed Multifunctional Hybrid Materials" (no. TQ05000001) is co-financed from the state budget by the Technology Agency of the Czech Republic under the SIGMA Programme within the M-ERA-NET 3 Call 2023. This project/result was funded under the National Recovery Plan from the European Recovery and Resilience Facility.

References

1 N. K. Chaudhari, H. Jin, B. Kim, D. San Baek, S. H. Joo and K. Lee, MXene: An Emerging Two-Dimensional Material for Future Energy Conversion and Storage Applications, *J. Mater. Chem. A*, 2017, **5**(47), 24564–24579, DOI: **10.1039/C7TA09094C**.

2 Y. Zhao, G. I. N. Waterhouse, G. Chen, X. Xiong, L.-Z. Wu, C.-H. Tung and T. Zhang, Two-Dimensional-Related Catalytic Materials for Solar-Driven Conversion of CO_x into Valuable Chemical Feedstocks, *Chem. Soc. Rev.*, 2019, **48**(7), 1972–2010, DOI: **10.1039/C8CS00607E**.

3 P. Miró, M. Audiffred and T. Heine, An Atlas of Two-Dimensional Materials, *Chem. Soc. Rev.*, 2014, **43**(18), 6537–6554, DOI: **10.1039/C4CS00102H**.

4 G. R. Bhimanapati, Z. Lin, V. Meunier, Y. Jung, J. Cha, S. Das, D. Xiao, Y. Son, M. S. Strano, V. R. Cooper, L. Liang, S. G. Louie, E. Ringe, W. Zhou, S. S. Kim, R. R. Naik, B. G. Sumpter, H. Terrones, F. Xia, Y. Wang, J. Zhu, D. Akinwande, N. Alem, J. A. Schuller, R. E. Schaak, M. Terrones and J. A. Robinson, Recent Advances in Two-Dimensional Materials beyond Graphene, *ACS Nano*, 2015, **9**(12), 11509–11539, DOI: **10.1021/acsnano.5b05556**.

5 J. Kang, V. K. Sangwan, J. D. Wood and M. C. Hersam, Solution-Based Processing of Monodisperse Two-Dimensional Nanomaterials, *Acc. Chem. Res.*, 2017, **50**(4), 943–951, DOI: **10.1021/acs.accounts.6b00643**.

6 S. Z. Butler, S. M. Hollen, L. Cao, Y. Cui, J. A. Gupta, H. R. Gutiérrez, T. F. Heinz, S. S. Hong, J. Huang, A. F. Ismach, E. Johnston-Halperin, M. Kuno, V. V. Plashnitsa, R. D. Robinson, R. S. Ruoff, S. Salahuddin, J. Shan, L. Shi, M. G. Spencer, M. Terrones, W. Windl and J. E. Goldberger, Progress, Challenges, and Opportunities in Two-Dimensional Materials Beyond Graphene, *ACS Nano*, 2013, **7**(4), 2898–2926, DOI: **10.1021/nn400280c**.

7 S. Bellani, A. Bartolotta, A. Agresti, G. Calogero, G. Grancini, A. Di Carlo, E. Kymakis and F. Bonaccorso, Solution-Processed Two-Dimensional Materials for next-Generation Photovoltaics, *Chem. Soc. Rev.*, 2021, **50**(21), 11870–11965, DOI: **10.1039/D1CS00106J**.

8 F. Liu and Z. Fan, Defect Engineering of Two-Dimensional Materials for Advanced Energy Conversion and Storage, *Chem. Soc. Rev.*, 2023, **52**(5), 1723–1772, DOI: **10.1039/D2CS00931E**.

9 X. Wang, Q. Weng, Y. Yang, Y. Bando and D. Golberg, Hybrid Two-Dimensional Materials in Rechargeable Battery Applications and Their Microscopic Mechanisms, *Chem. Soc. Rev.*, 2016, **45**(15), 4042–4073, DOI: **10.1039/C5CS00937E**.

10 Z. Cai, B. Liu, X. Zou and H.-M. Cheng, Chemical Vapor Deposition Growth and Applications of Two-Dimensional Materials and Their Heterostructures, *Chem. Rev.*, 2018, **118**(13), 6091–6133, DOI: **10.1021/acs.chemrev.7b00536**.

11 A. K. Mishra, K. V. Lakshmi and L. Huang, Eco-Friendly Synthesis of Metal Dichalcogenides Nanosheets and Their Environmental Remediation Potential Driven by Visible Light, *Sci. Rep.*, 2015, **5**(1), 15718, DOI: **10.1038/srep15718**.

12 Q. Cai, L. H. Li, S. Mateti, A. Bhattacharjee, Y. Fan, S. Huang and Y. I. Chen, Boron Nitride Nanosheets: Thickness-Related Properties and Applications, *Adv. Funct. Mater.*, 2024, **34**, 2403669, DOI: **10.1002/adfm.202403669**.

13 T. Chu, D. Liu, Y. Tian, Y. Li, W. Liu, G. Li, Z. Song, Z. Jian and X. Cai, Cationic Hexagonal Boron Nitride, Graphene, and MoS2Nanosheets Heteroassembled with Their

Anionic Counterparts for Photocatalysis and Sodium-Ion Battery Applications, *ACS Appl. Nano Mater.*, 2020, **3**(6), 5327–5334, DOI: **10.1021/acsanm.0c00700**.

14 M. K. Mohanta, T. K. Sahu, D. Gogoi, N. R. Peela and M. Qureshi, Hexagonal Boron Nitride Quantum Dots as a Superior Hole Extractor for Efficient Charge Separation in WO3-Based Photoelectrochemical Water Oxidation, *ACS Appl. Energy Mater.*, 2019, **2**(10), 7457–7466, DOI: **10.1021/acsaem.9b01450**.

15 P. T. Araujo, M. Terrones and M. S. Dresselhaus, Defects and Impurities in Graphene-like Materials, *Mater. Today*, 2012, **15**(3), 98–109, DOI: **10.1016/S1369-7021(12)70045-7**.

16 Q. Xiang, J. Yu and M. Jaroniec, Graphene-Based Semiconductor Photocatalysts, *Chem. Soc. Rev.*, 2012, **41**(2), 782–796, DOI: **10.1039/C1CS15172J**.

17 M. Pumera, Graphene-Based Nanomaterials for Energy Storage, *Energy Environ. Sci.*, 2011, **4**(3), 668–674, DOI: **10.1039/C0EE00295J**.

18 C. Liu, Z. Yu, D. Neff, A. Zhamu and B. Z. Jang, Graphene-Based Supercapacitor with an Ultrahigh Energy Density, *Nano Lett.*, 2010, **10**(12), 4863–4868, DOI: **10.1021/nl102661q**.

19 R. Ye, D. K. James and J. M. Tour, Laser-Induced Graphene: From Discovery to Translation, *Adv. Mater.*, 2019, **31**(1), 1803621, DOI: **10.1002/adma.201803621**.

20 M. Romagnoli, V. Sorianello, M. Midrio, F. H. L. Koppens, C. Huyghebaert, D. Neumaier, P. Galli, W. Templ, A. D'Errico and A. C. Ferrari, Graphene-Based Integrated Photonics for next-Generation Datacom and Telecom, *Nat. Rev. Mater.*, 2018, **3**(10), 392–414, DOI: **10.1038/s41578-018-0040-9**.

21 X.-Y. Wang, A. Narita and K. Müllen, Precision Synthesis versus Bulk-Scale Fabrication of Graphenes, *Nat. Rev. Chem.*, 2017, **2**(1), 0100, DOI: **10.1038/s41570-017-0100**.

22 C. Yang, C. Yang, Y. Guo, J. Feng and X. Guo, Graphene–Molecule–Graphene Single-Molecule Junctions to Detect Electronic Reactions at the Molecular Scale, *Nat. Protoc.*, 2023, **18**(6), 1958–1978, DOI: **10.1038/s41596-023-00822-x**.

23 R. Srivastava, S. Nouseen, J. Chattopadhyay, P. M. Woi, D. N. Son and B. P. Bastakoti, Recent Advances in Electrochemical Water Splitting and Reduction of CO_2 into Green Fuels on 2D Phosphorene-Based Catalyst, *Energy Technol.*, 2021, **9**(1), 2000741, DOI: **10.1002/ente.202000741**.

24 M. Batmunkh, M. Bat-Erdene and J. G. Shapter, Phosphorene and Phosphorene-Based Materials – Prospects for Future Applications, *Adv. Mater.*, 2016, **28**(39), 8586–8617, DOI: **10.1002/adma.201602254**.

25 A. Carvalho, M. Wang, X. Zhu, A. S. Rodin, H. Su and A. H. Castro Neto, Phosphorene: From Theory to Applications, *Nat. Rev. Mater.*, 2016, **1**(11), 16061, DOI: **10.1038/natrevmats.2016.61**.

26 M. Shao, F. Ning, M. Wei, D. G. Evans and X. Duan, Hierarchical Nanowire Arrays Based on ZnO Core-Layered Double Hydroxide Shell for Largely Enhanced Photoelectrochemical Water Splitting, *Adv. Funct. Mater.*, 2014, **24**(5), 580–586, DOI: **10.1002/adfm.201301889**.

27 S. Xu, Y. Dall'Agnese, G. Wei, C. Zhang, Y. Gogotsi and W. Han, Screen-Printable Microscale Hybrid Device Based on MXene and Layered Double Hydroxide Electrodes for Powering Force Sensors, *Nano Energy*, 2018, **50**, 479–488, DOI: **10.1016/j.nanoen.2018.05.064**.

28 A. G, N. Gupta, P. Saha and P. Bhattacharya, 3D Printing of MXenes-Based Electrodes for Energy Storage Applications, *Recent Prog. Mater.*, 2023, **05**(02), 1–23, DOI: **10.21926/rpm.2302020**.

29 N. A. Shepelin, P. C. Sherrell, E. N. Skountzos, E. Goudeli, J. Zhang, V. C. Lussini, B. Imtiaz, K. A. S. Usman, G. W. Dicinoski, J. G. Shapter, J. M. Razal and A. V. Ellis, Interfacial Piezoelectric Polarization Locking in Printable Ti3C2Tx MXene-Fluoropolymer Composites, *Nat. Commun.*, 2021, **12**(1), DOI: **10.1038/s41467-021-23341-3**.

30 Q. Jiang, N. Kurra, M. Alhabeb, Y. Gogotsi and H. N. Alshareef, All Pseudocapacitive MXene-RuO_2 Asymmetric Supercapacitors, *Adv. Energy Mater.*, 2018, **8**(13), 1703043, DOI: **10.1002/aenm.201703043**.

31 J. L. Hart, K. Hantanasirisakul, A. C. Lang, B. Anasori, D. Pinto, Y. Pivak, J. T. van Omme, S. J. May, Y. Gogotsi and M. L. Taheri, Control of MXenes' Electronic Properties through Termination and Intercalation, *Nat. Commun.*, 2019, **10**(1), 522, DOI: **10.1038/s41467-018-08169-8**.

32 A. S. Levitt, M. Alhabeb, C. B. Hatter, A. Sarycheva, G. Dion and Y. Gogotsi, Electrospun MXene/Carbon Nanofibers as Supercapacitor Electrodes, *J. Mater. Chem. A*, 2019, **7**(1), 269–277, DOI: **10.1039/C8TA09810G**.

33 B. K. Deka, A. Hazarika, G. H. Kang, Y. J. Hwang, A. P. Jaiswal, D. Chan Kim, Y. B. Park and H. W. Park, 3D-Printed Structural Supercapacitor with MXene-N@Zn-Co Selenide Nanowire Based Woven Carbon Fiber Electrodes, *ACS Energy Lett.*, 2023, **8**(2), 963–971, DOI: **10.1021/acsenergylett.2c02505**.

34 S. Nouseen and M. Pumera, MXene 3D/4D Printing: Ink Formulation and Electrochemical Energy Storage Applications, *Adv. Funct. Mater.*, 2025, 2421987, DOI: **10.1002/adfm.202421987**.

35 S. Nouseen, S. Deshmukh and M. Pumera, Nanoarchitectonics of Laser Induced MAX 3D-Printed Electrode for Photo-Electrocatalysis and Energy Storage Application with Long Cyclic Durability of 100 000 Cycles, *Adv. Funct. Mater.*, 2024, **34**(45), 2407071, DOI: **10.1002/adfm.202407071**.

36 S. Nouseen, K. Ghosh and M. Pumera, Hydrofluoric Acid-Free Etched MAX on 3D-Printed Nanocarbon Electrode for Photoelectrochemical Hydrogen Production, *Appl. Mater. Today*, 2024, **36**, 101995, DOI: **10.1016/j.apmt.2023.101995**.

37 S. Nouseen, K. Ghosh and M. Pumera, 3D Printing of MAX/PLA Filament: Electrochemical in-Situ Etching for Enhanced Energy Conversion and Storage, *Electrochem. Commun.*, 2023, 107652, DOI: **10.1016/j.elecom.2023.107652**.

38 L. Wang, M. Han, C. E. Shuck, X. Wang and Y. Gogotsi, Adjustable Electrochemical Properties of Solid-Solution

MXenes, *Nano Energy*, 2021, **88**, 106308, DOI: 10.1016/j.nanoen.2021.106308.

39 M. Han, K. Maleski, C. E. Shuck, Y. Yang, J. T. Glazar, A. C. Foucher, K. Hantanasirisakul, A. Sarycheva, N. C. Frey, S. J. May, V. B. Shenoy, E. A. Stach and Y. Gogotsi, Tailoring Electronic and Optical Properties of MXenes through Forming Solid Solutions, *J. Am. Chem. Soc.*, 2020, **142**(45), 19110–19118, DOI: 10.1021/jacs.0c07395.

40 X.-H. Zha, Q. Huang, J. He, H. He, J. Zhai, J. S. Francisco and S. Du, The Thermal and Electrical Properties of the Promising Semiconductor MXene Hf2CO2, *Sci. Rep.*, 2016, **6**(1), 27971, DOI: 10.1038/srep27971.

41 C. E. Shuck, M. Han, K. Maleski, K. Hantanasirisakul, S. J. Kim, J. Choi, W. E. B. Reil and Y. Gogotsi, Effect of Ti3AlC2 MAX Phase on Structure and Properties of Resultant Ti3C2Tx MXene, *ACS Appl. Nano Mater.*, 2019, **2**(6), 3368–3376, DOI: 10.1021/acsanm.9b00286.

42 K. Maleski, C. E. Ren, M.-Q. Zhao, B. Anasori and Y. Gogotsi, Size-Dependent Physical and Electrochemical Properties of Two-Dimensional MXene Flakes, *ACS Appl. Mater. Interfaces*, 2018, **10**(29), 24491–24498, DOI: 10.1021/acsami.8b04662.

43 T. Schultz, N. C. Frey, K. Hantanasirisakul, S. Park, S. J. May, V. B. Shenoy, Y. Gogotsi and N. Koch, Surface Termination Dependent Work Function and Electronic Properties of $Ti_3C_2T_x$ MXene, *Chem. Mater.*, 2019, **31**(17), 6590–6597, DOI: 10.1021/acs.chemmater.9b00414.

44 G. Zhu, H. Zhang, J. Lu, Y. Hou, P. Liu, S. Dong, H. Pang and Y. Zhang, 3D Printing of MXene-Enhanced Ferroelectric Polymer for Ultrastable Zinc Anodes, *Adv. Funct. Mater.*, 2024, **34**(1), 2305550, DOI: 10.1002/adfm.202305550.

45 Z. Yu, L. Jiang, R. Liu, W. Zhao, Z. Yang, J. Zhang and S. Jin, Versatile Self-Assembled MXene-Au Nanocomposites for SERS Detection of Bacteria, Antibacterial and Photothermal Sterilization, *Chem. Eng. J.*, 2021, **426**, 131914, DOI: 10.1016/j.cej.2021.131914.

46 L. Li, J. Meng, X. Bao, Y. Huang, X. Yan, H. Qian, C. Zhang and T. Liu, Direct-Ink-Write 3D Printing of Programmable Micro-Supercapacitors from MXene-Regulating Conducting Polymer Inks, *Adv. Energy Mater.*, 2023, **13**(9), 2203683, DOI: 10.1002/aenm.202203683.

47 Y. Song, Y. Xu, Q. Guo, Z. Hua, F. Yin and W. Yuan, MXene-Derived TiO2Nanoparticles Intercalating between RGO Nanosheets: An Assembly for Highly Sensitive Gas Detection, *ACS Appl. Mater. Interfaces*, 2021, **13**(33), 39772–39780, DOI: 10.1021/acsami.1c12154.

48 Z. Wang, S. Qin, S. Seyedin, J. Zhang, J. Wang, A. Levitt, N. Li, C. Haines, R. Ovalle-Robles, W. Lei, Y. Gogotsi, R. H. Baughman and J. M. Razal, High-Performance Biscrolled MXene/Carbon Nanotube Yarn Supercapacitors, *Small*, 2018, **14**(37), 1802225, DOI: 10.1002/smll.201802225.

49 U. Amara, I. Hussain, M. Ahmad, K. Mahmood and K. Zhang, 2D MXene-Based Biosensing: A Review, *Small*, 2023, **19**(2), 2205249, DOI: 10.1002/smll.202205249.

50 M. Zhao, C. E. Ren, Z. Ling, M. R. Lukatskaya, C. Zhang, K. L. Van Aken, M. W. Barsoum and Y. Gogotsi, Flexible MXene/Carbon Nanotube Composite Paper with High Volumetric Capacitance, *Adv. Mater.*, 2015, **27**(2), 339–345, DOI: 10.1002/adma.201404140.

51 M. Naguib, M. Kurtoglu, V. Presser, J. Lu, J. Niu, M. Heon, L. Hultman, Y. Gogotsi and M. W. Barsoum, Two-Dimensional Nanocrystals Produced by Exfoliation of Ti_3AlC_2, *Adv. Mater.*, 2011, **23**(37), 4248–4253, DOI: 10.1002/adma.201102306.

52 X. Li, Z. Huang, C. E. Shuck, G. Liang, Y. Gogotsi and C. Zhi, MXene Chemistry, Electrochemistry and Energy Storage Applications, *Nat. Rev. Chem.*, 2022, **6**(6), 389–404, DOI: 10.1038/s41570-022-00384-8.

53 J. Li, C. Wang, Z. Yu, Y. Chen and L. Wei, MXenes for Zinc-Based Electrochemical Energy Storage Devices, *Small*, 2023, **20**(39), 2304543, DOI: 10.1002/smll.202304543.

54 B. Anasori, M. R. Lukatskaya and Y. Gogotsi, 2D Metal Carbides and Nitrides (MXenes) for Energy Storage, *Nat. Rev. Mater.*, 2017, **2**(2), 16098, DOI: 10.1038/natrevmats.2016.98.

55 J. Nan, X. Guo, J. Xiao, X. Li, W. Chen, W. Wu, H. Liu, Y. Wang, M. Wu and G. Wang, Nanoengineering of 2D MXene-Based Materials for Energy Storage Applications, *Small*, 2021, **17**(9), 1902085, DOI: 10.1002/smll.201902085.

56 K. Li, M. Liang, H. Wang, X. Wang, Y. Huang, J. Coelho, S. Pinilla, Y. Zhang, F. Qi, V. Nicolosi and Y. Xu, 3D MXene Architectures for Efficient Energy Storage and Conversion, *Adv. Funct. Mater.*, 2020, **30**(47), 2000842, DOI: 10.1002/adfm.202000842.

57 Y. A. Kumar, N. Roy, T. Ramachandran, M. Hussien, M. Moniruzzaman and S. W. Joo, Shaping the Future of Energy: The Rise of Supercapacitors Progress in the Last Five Years, *J. Energy Storage*, 2024, **98**, 113040, DOI: 10.1016/j.est.2024.113040.

58 Y. Anil Kumar, S. Vignesh, T. Ramachandran, A. M. Fouda, H. H. Hegazy, M. Moniruzzaman and T. Hwan Oh, Advancements in Novel Electrolyte Materials: Pioneering the Future of Supercapacitive Energy Storage, *J. Ind. Eng. Chem.*, 2025, **145**, 191–215, DOI: 10.1016/j.jiec.2024.11.018.

59 T. Ramachandran, R. K. Raji, S. Palanisamy, N. Renuka and K. Karuppasamy, The Role of in Situ and Operando Techniques in Unraveling Local Electrochemical Supercapacitor Phenomena, *J. Ind. Eng. Chem.*, 2025, **145**, 144–168, DOI: 10.1016/j.jiec.2024.10.077.

60 Y. A. Kumar, J. K. Alagarasan, T. Ramachandran, M. Rezeq, M. A. Bajaber, A. A. Alalwiat, M. Moniruzzaman and M. Lee, The Landscape of Energy Storage: Insights into Carbon Electrode Materials and Future Directions, *J. Energy Storage*, 2024, **86**, 111119, DOI: 10.1016/j.est.2024.111119.

61 N. Roy, Y. Anil Kumar, T. Ramachandran, A. M. Fouda, H. H. Hegazy, M. Moniruzzaman and S. Woo Joo, Biomass-Derived Nanostructures and Hydrothermal Carbon Spheres: A Review of Electrochemical Applications in Redox Flow Battery, *J. Ind. Eng. Chem.*, 2025, **144**, 228–254, DOI: 10.1016/j.jiec.2024.10.017.

62 T. Ramachandran, N. Roy, H. H. Hegazy, I. S. Yahia, Y. A. Kumar, M. Moniruzzaman and S. W. Joo, From Graphene Aerogels to Efficient Energy Storage: Current

Developments and Future Prospects, *J. Alloys Compd.*, 2025, **1010**, 177248, DOI: 10.1016/j.jallcom.2024.177248.

63 J. Pang, R. G. Mendes, A. Bachmatiuk, L. Zhao, H. Q. Ta, T. Gemming, H. Liu, Z. Liu and M. H. Rummeli, Applications of 2D MXenes in Energy Conversion and Storage Systems, *Chem. Soc. Rev.*, 2019, **48**(1), 72–133, DOI: 10.1039/C8CS00324F.

64 Y. Zhong, X. Xia, F. Shi, J. Zhan, J. Tu and H. J. Fan, Transition Metal Carbides and Nitrides in Energy Storage and Conversion, *Adv. Sci.*, 2016, **3**(5), 1500286, DOI: 10.1002/advs.201500286.

65 L. Tang, X. Meng, D. Deng and X. Bao, Confinement Catalysis with 2D Materials for Energy Conversion, *Adv. Mater.*, 2019, **31**(50), 1901996, DOI: 10.1002/adma.201901996.

66 J. Pang, B. Chang, H. Liu and W. Zhou, Potential of MXene-Based Heterostructures for Energy Conversion and Storage, *ACS Energy Lett.*, 2022, **14**, 78–96, DOI: 10.1021/acsenergylett.1c02132.

67 X. Hui, X. Ge, R. Zhao, Z. Li and L. Yin, Interface Chemistry on MXene-Based Materials for Enhanced Energy Storage and Conversion Performance, *Adv. Funct. Mater.*, 2020, **30**(50), 2005190, DOI: 10.1002/adfm.202005190.

68 C. Anichini, W. Czepa, D. Pakulski, A. Aliprandi, A. Ciesielski and P. Samorì, Chemical Sensing with 2D Materials, *Chem. Soc. Rev.*, 2018, **47**(13), 4860–4908, DOI: 10.1039/C8CS00417J.

69 L. Li, S. Zhao, X.-J. Luo, H.-B. Zhang and Z.-Z. Yu, Smart MXene-Based Janus Films with Multi-Responsive Actuation Capability and High Electromagnetic Interference Shielding Performances, *Carbon*, 2021, **175**, 594–602, DOI: 10.1016/j.carbon.2020.10.090.

70 S. Zhao, H.-B. Zhang, J.-Q. Luo, Q.-W. Wang, B. Xu, S. Hong and Z.-Z. Yu, Highly Electrically Conductive Three-Dimensional $Ti_3C_2T_x$ MXene/Reduced Graphene Oxide Hybrid Aerogels with Excellent Electromagnetic Interference Shielding Performances, *ACS Nano*, 2018, **12**(11), 11193–11202, DOI: 10.1021/acsnano.8b05739.

71 W. Yuan, H. Liu, X. Wang, L. Huang, F. Yin and Y. Yuan, Conductive MXene/Melamine Sponge Combined with 3D Printing Resin Base Prepared as an Electromagnetic Interferences Shielding Switch, *Composites, Part A*, 2021, **143**, 106238, DOI: 10.1016/j.compositesa.2020.106238.

72 Y. Zhao, J. Zhang, X. Guo, X. Cao, S. Wang, H. Liu and G. Wang, Engineering Strategies and Active Site Identification of MXene-Based Catalysts for Electrochemical Conversion Reactions, *Chem. Soc. Rev.*, 2023, **52**(9), 3215–3264, DOI: 10.1039/D2CS00698G.

73 X. Gao and E. C. M. Tse, Unraveling the Performance Descriptors for Designing Single-Atom Catalysts on Defective MXenes for Exclusive Nitrate-To-Ammonia Electrocatalytic Upcycling, *Small*, 2024, **20**(11), 2306311, DOI: 10.1002/smll.202306311.

74 F. Wang, S. Jin, Y. Du, Q. Xia, L. Wang and A. Zhou, Preparation of Mo2CT MXene as Co-Catalyst for H2 Production by Etching of Pure/Mixed HBr Solution, *Diam. Relat. Mater.*, 2023, **136**, 109922, DOI: 10.1016/j.diamond.2023.109922.

75 B. Lu, Z. Zhu, B. Ma, W. Wang, R. Zhu and J. Zhang, 2D MXene Nanomaterials for Versatile Biomedical Applications: Current Trends and Future Prospects, *Small*, 2021, **17**(46), 2100946, DOI: 10.1002/smll.202100946.

76 S. P. Sreenilayam, I. Ul Ahad, V. Nicolosi and D. Brabazon, MXene Materials Based Printed Flexible Devices for Healthcare, Biomedical and Energy Storage Applications, *Mater. Today*, 2021, **43**, 99–131, DOI: 10.1016/j.mattod.2020.10.025.

77 Y. Cai, X. Chen, Y. Xu, Y. Zhang, H. Liu, H. Zhang and J. Tang, $Ti_3C_2T_x$ MXene/Carbon Composites for Advanced Supercapacitors: Synthesis, Progress, and Perspectives, *Carbon Energy*, 2024, **6**(2), 2100946, DOI: 10.1002/cey2.501.

78 M. Naguib, V. N. Mochalin, M. W. Barsoum and Y. Gogotsi, 25th Anniversary Article: MXenes: A New Family of Two-Dimensional Materials, *Adv. Mater.*, 2014, **26**(7), 992–1005, DOI: 10.1002/adma.201304138.

79 M. Naguib, O. Mashtalir, J. Carle, V. Presser, J. Lu, L. Hultman, Y. Gogotsi and M. W. Barsoum, Two-Dimensional Transition Metal Carbides, *ACS Nano*, 2012, **6**(2), 1322–1331, DOI: 10.1021/nn204153h.

80 A. Thakur, B. S. N. Chandran, K. Davidson, A. Bedford, H. Fang, Y. Im, V. Kanduri, B. C. Wyatt, S. K. Nemani, V. Poliukhova, R. Kumar, Z. Fakhraai and B. Anasori, Step-by-Step Guide for Synthesis and Delamination of $Ti_3C_2T_x$ MXene, *Small Methods*, 2023, **7**(8), 2300030, DOI: 10.1002/smtd.202300030.

81 J. Mei, G. A. Ayoko, C. Hu and Z. Sun, Thermal Reduction of Sulfur-Containing MAX Phase for MXene Production, *Chem. Eng. J.*, 2020, **395**, 125111, DOI: 10.1016/j.cej.2020.125111.

82 T. S. Mathis, K. Maleski, A. Goad, A. Sarycheva, M. Anayee, A. C. Foucher, K. Hantanasirisakul, C. E. Shuck, E. A. Stach and Y. Gogotsi, Modified MAX Phase Synthesis for Environmentally Stable and Highly Conductive Ti3C2MXene, *ACS Nano*, 2021, **15**(4), 6420–6429, DOI: 10.1021/acsnano.0c08357.

83 M. Downes, C. E. Shuck, B. McBride, J. Busa and Y. Gogotsi, Comprehensive Synthesis of Ti3C2Tx from MAX Phase to MXene, *Nat. Protoc.*, 2024, **19**(6), 1807–1834, DOI: 10.1038/s41596-024-00969-1.

84 Y. Gogotsi, The Future of MXenes, *Chem. Mater.*, 2023, **35**(21), 8767–8770, DOI: 10.1021/acs.chemmater.3c02491.

85 B. Anasori and Y. Gogotsi, MXenes: Trends, Growth, and Future Directions, *Graphene 2D Mater.*, 2022, **7**(3–4), 75–79, DOI: 10.1007/s41127-022-00053-z.

86 A. Ghosh, H. Pal, T. Das, S. Chatterjee and A. Das, Synthesis and Characterization of MXene from MAX Phase, *Mater. Today Proc.*, 2022, **58**, 714–716, DOI: 10.1016/j.matpr.2022.02.253.

87 J. L. Hart, K. Hantanasirisakul, A. C. Lang, B. Anasori, D. Pinto, Y. Pivak, J. T. van Omme, S. J. May, Y. Gogotsi and M. L. Taheri, Control of MXenes' Electronic Properties through Termination and Intercalation, *Nat.*

Commun., 2019, **10**(1), 522, DOI: 10.1038/s41467-018-08169-8.

88 A. Miranda, J. Halim, M. W. Barsoum and A. Lorke, Electronic Properties of Freestanding Ti3C2Tx MXene Monolayers, *Appl. Phys. Lett.*, 2016, **108**(3), DOI: 10.1063/1.4939971.

89 Z. Lin, D. Barbara, P.-L. Taberna, K. L. Van Aken, B. Anasori, Y. Gogotsi and P. Simon, Capacitance of Ti3C2Tx MXene in Ionic Liquid Electrolyte, *J. Power Sources*, 2016, **326**, 575–579, DOI: 10.1016/j.jpowsour.2016.04.035.

90 S. Park, Y.-L. Lee, Y. Yoon, S. Y. Park, S. Yim, W. Song, S. Myung, K.-S. Lee, H. Chang, S. S. Lee and K.-S. An, Reducing the High Hydrogen Binding Strength of Vanadium Carbide MXene with Atomic Pt Confinement for High Activity toward HER, *Appl. Catal., B*, 2022, **304**, 120989, DOI: 10.1016/j.apcatb.2021.120989.

91 M. Pramanik, M. V. Limaye, M. S. Pawar, D. J. Late and S. B. Singh, Post-Ammonia-Treated V_2CT_x MXene at Different Pressures: Effects on Morphology, Electronic, and Optical Properties, *J. Phys. Chem. C*, 2023, **127**(9), 4609–4617, DOI: 10.1021/acs.jpcc.2c08083.

92 S. Kwon, J. Lee, Y. I. Jhon, G. Lim, Y. M. Jhon and J. H. Lee, Photothermal Property Investigation of V2CTx MXene and Its Use for All-Optical Modulator, *Opt. Mater.*, 2022, **134**, 113198, DOI: 10.1016/j.optmat.2022.113198.

93 Y. Liu, J. Zhang, X. Zhang, Y. Li and J. Wang, $Ti_3C_2T_x$ Filler Effect on the Proton Conduction Property of Polymer Electrolyte Membrane, *ACS Appl. Mater. Interfaces*, 2016, **8**(31), 20352–20363, DOI: 10.1021/acsami.6b04800.

94 X. Zhai, H. Dong, Y. Li, X. Yang, L. Li, J. Yang, Y. Zhang, J. Zhang, H. Yan and G. Ge, Termination Effects of Single-Atom Decorated v-Mo2CTx MXene for the Electrochemical Nitrogen Reduction Reaction, *J. Colloid Interface Sci.*, 2022, **605**, 897–905, DOI: 10.1016/j.jcis.2021.07.083.

95 J. Liang, C. Ding, J. Liu, T. Chen, W. Peng, Y. Li, F. Zhang and X. Fan, Heterostructure Engineering of Co-Doped MoS_2 Coupled with Mo_2CT_x MXene for Enhanced Hydrogen Evolution in Alkaline Media, *Nanoscale*, 2019, **11**(22), 10992–11000, DOI: 10.1039/C9NR02085C.

96 W. Guo, S. G. Surya, V. Babar, F. Ming, S. Sharma, H. N. Alshareef, U. Schwingenschlögl and K. N. Salama, Selective Toluene Detection with Mo_2CT_x MXene at Room Temperature, *ACS Appl. Mater. Interfaces*, 2020, **12**(51), 57218–57227, DOI: 10.1021/acsami.0c16302.

97 K. Zhu, Y. Jin, F. Du, S. Gao, Z. Gao, X. Meng, G. Chen, Y. Wei and Y. Gao, Synthesis of Ti2CT MXene as Electrode Materials for Symmetric Supercapacitor with Capable Volumetric Capacitance, *J. Energy Chem.*, 2019, **31**, 11–18, DOI: 10.1016/j.jechem.2018.03.010.

98 S. A. Melchior, N. Palaniyandy, I. Sigalas, S. E. Iyuke and K. I. Ozoemena, Probing the Electrochemistry of MXene (Ti2CTx)/Electrolytic Manganese Dioxide (EMD) Composites as Anode Materials for Lithium-Ion Batteries, *Electrochim. Acta*, 2019, **297**, 961–973, DOI: 10.1016/j.electacta.2018.12.013.

99 A. D. Dillon, M. J. Ghidiu, A. L. Krick, J. Griggs, S. J. May, Y. Gogotsi, M. W. Barsoum and A. T. Fafarman, Highly Conductive Optical Quality Solution-Processed Films of 2D Titanium Carbide, *Adv. Funct. Mater.*, 2016, **26**(23), 4162–4168, DOI: 10.1002/adfm.201600357.

100 M. Ghidiu, M. R. Lukatskaya, M.-Q. Zhao, Y. Gogotsi and M. W. Barsoum, Conductive Two-Dimensional Titanium Carbide 'Clay' with High Volumetric Capacitance, *Nature*, 2014, **516**(7529), 78–81, DOI: 10.1038/nature13970.

101 V. Kotasthane, Z. Tan, J. Yun, E. B. Pentzer, J. L. Lutkenhaus, M. J. Green and M. Radovic, Selective Etching of Ti_3AlC_2 MAX Phases Using Quaternary Ammonium Fluorides Directly Yields $Ti_3C_2T_z$ MXene Nanosheets: Implications for Energy Storage, *ACS Appl. Nano Mater.*, 2023, **6**(2), 1093–1105, DOI: 10.1021/acsanm.2c04607.

102 Y. Gogotsi, Monolithic Integrated MXene Supercapacitors May Power Future Electronics, *Natl. Sci. Rev.*, 2023, **10**(3), nwad020, DOI: 10.1093/nsr/nwad020.

103 Y. Gogotsi and Q. Huang, MXenes: Two-Dimensional Building Blocks for Future Materials and Devices, *ACS Nano*, 2021, **15**(4), 5775–5780, DOI: 10.1021/acsnano.1c03161.

104 X. Xie and N. Zhang, Positioning MXenes in the Photocatalysis Landscape: Competitiveness, Challenges, and Future Perspectives, *Adv. Funct. Mater.*, 2020, **30**(36), 2002528, DOI: 10.1002/adfm.202002528.

105 Y. Zhu, S. Wang, J. Ma, P. Das, S. Zheng and Z.-S. Wu, Recent Status and Future Perspectives of 2D MXene for Micro-Supercapacitors and Micro-Batteries, *Energy Storage Mater.*, 2022, **51**, 500–526, DOI: 10.1016/j.ensm.2022.06.044.

106 C. Lamiel, I. Hussain, J. H. Warner and K. Zhang, Beyond Ti-Based MXenes: A Review of Emerging Non-Ti Based Metal-MXene Structure, Properties, and Applications, *Mater. Today*, 2023, **63**, 313–338, DOI: 10.1016/j.mattod.2023.01.020.

107 P. Urbankowski, B. Anasori, T. Makaryan, D. Er, S. Kota, P. L. Walsh, M. Zhao, V. B. Shenoy, M. W. Barsoum and Y. Gogotsi, Synthesis of Two-Dimensional Titanium Nitride Ti_4N_3 (MXene), *Nanoscale*, 2016, **8**(22), 11385–11391, DOI: 10.1039/C6NR02253G.

108 O. Mashtalir, M. Naguib, V. N. Mochalin, Y. Dall'Agnese, M. Heon, M. W. Barsoum and Y. Gogotsi, Intercalation and Delamination of Layered Carbides and Carbonitrides, *Nat. Commun.*, 2013, **4**(1), 1716, DOI: 10.1038/ncomms2664.

109 M. Naguib, R. R. Unocic, B. L. Armstrong and J. Nanda, Large-Scale Delamination of Multi-Layers Transition Metal Carbides and Carbonitrides "MXenes.", *Dalton Trans.*, 2015, **44**(20), 9353–9358, DOI: 10.1039/C5DT01247C.

110 T. Bashir, S. Zhou, S. Yang, S. A. Ismail, T. Ali, H. Wang, J. Zhao and L. Gao, Progress in 3D-MXene Electrodes for Lithium/Sodium/Potassium/Magnesium/Zinc/Aluminum-Ion Batteries, *Electrochem. Energy Rev.*, 2023, **63**(1), DOI: 10.1007/s41918-022-00174-2.

111 C. Zhang, S. J. Kim, M. Ghidiu, M. Q. Zhao, M. W. Barsoum, V. Nicolosi and Y. Gogotsi, Layered Orthorhombic Nb2O5@Nb4C3Tx and TiO2@Ti3C2Tx Hierarchical Composites for High Performance Li-Ion Batteries, *Adv. Funct. Mater.*, 2016, **26**(23), 4143–4151, DOI: **10.1002/adfm.201600682**.

112 H. Dong, P. Xiao, N. Jin, B. Wang, Y. Liu and Z. Lin, Molten Salt Derived Nb $_2$ CT $_x$ MXene Anode for Li-ion Batteries, *ChemElectroChem*, 2021, **8**(5), 957–962, DOI: **10.1002/celc.202100142**.

113 M. Hu, H. Zhang, T. Hu, B. Fan, X. Wang and Z. Li, Emerging 2D MXenes for Supercapacitors: Status, Challenges and Prospects, *Chem. Soc. Rev.*, 2020, **49**(18), 6666–6693, DOI: **10.1039/D0CS00175A**.

114 H. Huang and W. Yang, MXene-Based Micro-Supercapacitors: Ink Rheology, Microelectrode Design and Integrated System, *ACS Nano*, 2024, **18**(6), 4651–4682, DOI: **10.1021/acsnano.3c10246**.

115 J. Halim, M. Lukatskaya, E. Zurich and K. M. Cook, MXene for Supercapacitors View Project MXenes View Project, **https://www.researchgate.net/publication/261445482**.

116 S. Pu, Z. Wang, Y. Xie, J. Fan, Z. Xu, Y. Wang, H. He, X. Zhang, W. Yang and H. Zhang, Origin and Regulation of Self-Discharge in MXene Supercapacitors, *Adv. Funct. Mater.*, 2023, **33**(8), 2208715, DOI: **10.1002/adfm.202208715**.

117 G. Zhou, M. Li, C. Liu, Q. Wu and C. Mei, 3D Printed Ti $_3$ C $_2$ T $_x$ MXene/Cellulose Nanofiber Architectures for Solid-State Supercapacitors: Ink Rheology, 3D Printability, and Electrochemical Performance, *Adv. Funct. Mater.*, 2022, **32**(14), 2109593, DOI: **10.1002/adfm.202109593**.

118 W. Yang, J. Yang, J. J. Byun, F. P. Moissinac, J. Xu, S. J. Haigh, M. Domingos, M. A. Bissett, R. A. W. Dryfe and S. Barg, 3D Printing of Freestanding MXene Architectures for Current-Collector-Free Supercapacitors, *Adv. Mater.*, 2019, **31**(37), 1902725, DOI: **10.1002/adma.201902725**.

119 C. Zhang, L. McKeon, M. P. Kremer, S.-H. Park, O. Ronan, A. Seral-Ascaso, S. Barwich, C. Ó. Coileáin, N. McEvoy, H. C. Nerl, B. Anasori, J. N. Coleman, Y. Gogotsi and V. Nicolosi, Additive-Free MXene Inks and Direct Printing of Micro-Supercapacitors, *Nat. Commun.*, 2019, **10**(1), 1795, DOI: **10.1038/s41467-019-09398-1**.

120 K. Li, X. Wang, S. Li, P. Urbankowski, J. Li, Y. Xu and Y. Gogotsi, An Ultrafast Conducting Polymer@MXene Positive Electrode with High Volumetric Capacitance for Advanced Asymmetric Supercapacitors, *Small*, 2020, **16**(4), 1906851, DOI: **10.1002/smll.201906851**.

121 Q. Yue, J. Sun, S. Chen, Y. Zhou, H. Li, Y. Chen, R. Zhang, G. Wei and Y. Kang, Hierarchical Mesoporous MXene-NiCoP Electrocatalyst for Water-Splitting, *ACS Appl. Mater. Interfaces*, 2020, **12**(16), 18570–18577, DOI: **10.1021/acsami.0c01303**.

122 W. Yang, H. Hou, Y. Yang, G. Ma, X. Zhan, H. Yang and W. Yang, MXene-Derived Anatase-TiO2/Rutile-TiO2/In2O3 Heterojunctions toward Efficient Hydrogen Evolution, *Colloids Surf., A*, 2022, **652**, 129881, DOI: **10.1016/j.colsurfa.2022.129881**.

123 S. A. Sergiienko, D. V. Lopes, G. Constantinescu, M. C. Ferro, N. D. Shchaerban, O. B. Tursunov, V. I. Shkepu, H. Pazniak, N. Y. Tabachkova, E. R. Castellón, J. R. Frade and A. V. Kovalevsky, MXene-Containing Composite Electrodes for Hydrogen Evolution: Material Design Aspects and Approaches for Electrode Fabrication, *Int. J. Hydrogen Energy*, 2021, **46**(21), 11636–11651, DOI: **10.1016/j.ijhydene.2021.01.041**.

124 A. Liu, Y. Liu, G. Liu, A. Zhang, Y. Cheng, Y. Li, L. Zhang, L. Wang, H. Zhou, J. Liu and H. Wang, Engineering of Surface Modified Ti3C2Tx MXene Based Dually Controlled Drug Release System for Synergistic Multitherapies of Cancer, *Chem. Eng. J.*, 2022, **448**, 137691, DOI: **10.1016/j.cej.2022.137691**.

125 M. A. Munir and S. Khalid, Focused Review on the Synthesis of Titanium Carbide MXene via Fluorine-Free Methods for Lithium-Ion Batteries, *Energy Fuels*, 2025, **39**(6), 2889–2915, DOI: **10.1021/acs.energyfuels.4c04303**.

126 M. Li, Y. Wang, T. Li, J. Li, L. Huang, Q. Liu, J. Gu and D. Zhang, Hierarchical Few-Layer Fluorine-Free Ti $_3$ C $_2$ T $_x$ (T = O, OH)/MoS $_2$ Hybrid for Efficient Electrocatalytic Hydrogen Evolution, *J. Mater. Chem. A*, 2021, **9**(2), 922–927, DOI: **10.1039/D0TA08762A**.

127 M. Lu, H. Li, W. Han, J. Chen, W. Shi, J. Wang, X.-M. Meng, J. Qi, H. Li, B. Zhang, W. Zhang and W. Zheng, 2D Titanium Carbide (MXene) Electrodes with Lower-F Surface for High Performance Lithium-Ion Batteries, *J. Energy Chem.*, 2019, **31**, 148–153, DOI: **10.1016/j.jechem.2018.05.017**.

128 X. Yu, X. Cai, H. Cui, S.-W. Lee, X.-F. Yu and B. Liu, Fluorine-Free Preparation of Titanium Carbide MXene Quantum Dots with High near-Infrared Photothermal Performances for Cancer Therapy, *Nanoscale*, 2017, **9**(45), 17859–17864, DOI: **10.1039/C7NR05997C**.

129 J. Xuan, Z. Wang, Y. Chen, D. Liang, L. Cheng, X. Yang, Z. Liu, R. Ma, T. Sasaki and F. Geng, Organic-Base-Driven Intercalation and Delamination for the Production of Functionalized Titanium Carbide Nanosheets with Superior Photothermal Therapeutic Performance, *Angew. Chem.*, 2016, **128**(47), 14789–14794, DOI: **10.1002/ange.201606643**.

130 S. F. Hansen, M. B. Nielsen, L. M. Skjolding, J. Kaur, N. Desivyana, F. Hermansson, J. Bird, S. Barg, A. Khort, I. Odnevall, B. Fadeel and R. Arvidsson, Maximizing the Safety and Sustainability of MXenes, *Sci. Rep.*, 2024, **14**(1), 31030, DOI: **10.1038/s41598-024-82063-w**.

131 C. E. Shuck, K. Ventura-Martinez, A. Goad, S. Uzun, M. Shekhirev and Y. Gogotsi, Safe Synthesis of MAX and MXene: Guidelines to Reduce Risk During Synthesis, *ACS Chem. Health Saf.*, 2021, **28**(5), 326–338, DOI: **10.1021/acs.chas.1c00051**.

132 M. Ostermann, M. Piljević, E. Akbari, P. Patil, V. Zahorodna, I. Baginskiy, O. Gogotsi, C. Gachot, M. Rodríguez Ripoll, M. Valtiner and P. Bilotto, Pulsed Electrochemical Exfoliation for an HF-Free Sustainable

MXene Synthesis, *Small*, 2025, **21**(22), 2500807, DOI: 10.1002/smll.202500807.

133 A. M. Amani, L. Tayebi, E. Vafa, M. Abbasi, A. Vaez, H. Kamyab, S. Chelliapan, M. J. Azizli and R. Bazargan-Lari, On the Horizon of Greener Pathways to Travel into a Greener Future Portal: Green MXenes, Environment-Friendly Synthesis, and Their Innovative Applications, *J. Clean. Prod.*, 2024, **436**, 140606, DOI: 10.1016/j.jclepro.2024.140606.

134 Z. Sun, M. Yuan, L. Lin, H. Yang, C. Nan, H. Li, G. Sun and X. Yang, Selective Lithiation–Expansion–Microexplosion Synthesis of Two-Dimensional Fluoride-Free Mxene, *ACS Mater. Lett.*, 2019, **1**(6), 628–632, DOI: 10.1021/acsmaterialslett.9b00390.

135 A. J. Y. Wong, K. R. G. Lim and Z. W. Seh, Fluoride-Free Synthesis and Long-Term Stabilization of MXenes, *J. Mater. Res.*, 2022, **37**(22), 3988–3997, DOI: 10.1557/s43578-022-00680-5.

136 S. Kumar, Fluorine-Free MXenes: Recent Advances, Synthesis Strategies, and Mechanisms, *Small*, 2024, **20**(16), 2308225, DOI: 10.1002/smll.202308225.

137 M. Ghidiu, M. R. Lukatskaya, M.-Q. Zhao, Y. Gogotsi and M. W. Barsoum, Conductive Two-Dimensional Titanium Carbide 'Clay' with High Volumetric Capacitance, *Nature*, 2014, **516**(7529), 78–81, DOI: 10.1038/nature13970.

138 A. Feng, Y. Yu, F. Jiang, Y. Wang, L. Mi, Y. Yu and L. Song, Fabrication and Thermal Stability of NH 4 HF 2 -Etched Ti 3 C 2 MXene, *Ceram. Int.*, 2017, **43**(8), 6322–6328, DOI: 10.1016/j.ceramint.2017.02.039.

139 A. Feng, Y. Yu, Y. Wang, F. Jiang, Y. Yu, L. Mi and L. Song, Two-Dimensional MXene Ti3C2 Produced by Exfoliation of Ti3AlC2, *Mater. Des.*, 2017, **114**, 161–166, DOI: 10.1016/j.matdes.2016.10.053.

140 A. Feng, Y. Yu, Y. Wang, F. Jiang, Y. Yu, L. Mi and L. Song, Two-Dimensional MXene Ti3C2 Produced by Exfoliation of Ti3AlC2, *Mater. Des.*, 2017, **114**, 161–166, DOI: 10.1016/j.matdes.2016.10.053.

141 J. Wu, Y. Wang, Y. Zhang, H. Meng, Y. Xu, Y. Han, Z. Wang, Y. Dong and X. Zhang, Highly Safe and Ionothermal Synthesis of Ti3C2 MXene with Expanded Interlayer Spacing for Enhanced Lithium Storage, *J. Energy Chem.*, 2020, **47**, 203–209, DOI: 10.1016/j.jechem.2019.11.029.

142 V. Gajdosova, L. Lorencova, M. Prochazka, M. Omastova, M. Micusik, S. Prochazkova, F. Kveton, M. Jerigova, D. Velic, P. Kasak and J. Tkac, Remarkable Differences in the Voltammetric Response towards Hydrogen Peroxide, Oxygen and Ru(NH3)63+ of Electrode Interfaces Modified with HF or LiF-HCl Etched Ti3C2Tx MXene, *Microchim. Acta*, 2020, **187**(1), 52, DOI: 10.1007/s00604-019-4049-6.

143 Y. Guo, S. Jin, L. Wang, P. He, Q. Hu, L.-Z. Fan and A. Zhou, Synthesis of Two-Dimensional Carbide Mo2CTx MXene by Hydrothermal Etching with Fluorides and Its Thermal Stability, *Ceram. Int.*, 2020, **46**(11), 19550–19556, DOI: 10.1016/j.ceramint.2020.05.008.

144 D. Wang, C. Zhou, A. S. Filatov, W. Cho, F. Lagunas, M. Wang, S. Vaikuntanathan, C. Liu, R. F. Klie and D. V. Talapin, Direct Synthesis and Chemical Vapor Deposition of 2D Carbide and Nitride MXenes, https://www.science.org.

145 K. C. Chan, X. Guan, T. Zhang, K. Lin, Y. Huang, L. Lei, Y. Georgantas, Y. Gogotsi, M. A. Bissett and I. A. Kinloch, The Fabrication of Ti $_3$ C $_2$ and Ti $_3$ CN MXenes by Electrochemical Etching, *J. Mater. Chem. A*, 2024, **12**(37), 25165–25175, DOI: 10.1039/D4TA03457K.

146 C. Zhang, C. Wu, L. Wang and G. Liu, Selective H $_2$ O $_2$ Electrosynthesis over Defective Carbon from Electrochemical Etching of Molybdenum Carbide, *ACS Appl. Mater. Interfaces*, 2023, **15**(1), 838–847, DOI: 10.1021/acsami.2c15467.

147 M. Sheng, X. Bin, Y. Yang, Y. Tang and W. Que, In Situ Electrosynthesis of MAX-Derived Electrocatalysts for Superior Hydrogen Evolution Reaction, *Small*, 2022, **18**(32), 2203471, DOI: 10.1002/smll.202203471.

148 S. Pang, W. Io and J. Hao, Facile Atomic-Level Tuning of Reactive Metal–Support Interactions in the Pt QDs@ HF-Free MXene Heterostructure for Accelerating PH-Universal Hydrogen Evolution Reaction, *Adv. Sci.*, 2021, **8**(22), 2102207, DOI: 10.1002/advs.202102207.

149 L. Zhao, Z. Wang, Y. Li, S. Wang, L. Wang, Z. Qi, Q. Ge, X. Liu and J. Z. Zhang, Designed Synthesis of Chlorine and Nitrogen Co-Doped Ti3C2 MXene Quantum Dots and Their Outstanding Hydroxyl Radical Scavenging Properties, *J. Mater. Sci. Technol.*, 2021, **78**, 30–37, DOI: 10.1016/j.jmst.2020.10.048.

150 S. Pang, W. Io, L. Wong, J. Zhao and J. Hao, Efficient Energy Conversion and Storage Based on Robust Fluoride-Free Self-Assembled 1D Niobium Carbide in 3D Nanowire Network, *Adv. Sci.*, 2020, **7**(10), 1903680, DOI: 10.1002/advs.201903680.

151 S. Li, X. Zou, Y. Hu, X. Lu, X. Xiong, Q. Xu, H. Cheng and Z. Zhou, Electrochemical Reduction of TiO $_2$/Al $_2$ O $_3$/C to Ti $_3$ AlC $_2$ and Its Derived Two-Dimensional (2D) Carbides, *J. Electrochem. Soc.*, 2018, **165**(3), E97–E107, DOI: 10.1149/2.0181803jes.

152 A. Jawaid, A. Hassan, G. Neher, D. Nepal, R. Pachter, W. J. Kennedy, S. Ramakrishnan and R. A. Vaia, Halogen Etch of Ti $_3$ AlC $_2$ MAX Phase for MXene Fabrication, *ACS Nano*, 2021, **15**(2), 2771–2777, DOI: 10.1021/acsnano.0c08630.

153 C. Wang, H. Shou, S. Chen, S. Wei, Y. Lin, P. Zhang, Z. Liu, K. Zhu, X. Guo, X. Wu, P. M. Ajayan and L. Song, HCl-Based Hydrothermal Etching Strategy toward Fluoride-Free MXenes, *Adv. Mater.*, 2021, **33**(27), 2101015, DOI: 10.1002/adma.202101015.

154 Y. Wang, B. Zhou, Q. Tang, Y. Yang, B. Pu, J. Bai, J. Xu, Q. Feng, Y. Liu and W. Yang, Ultrafast Synthesis of MXenes in Minutes via Low-Temperature Molten Salt Etching, *Adv. Mater.*, 2024, **36**(49), 2410736, DOI: 10.1002/adma.202410736.

155 F. Wang, F. Tian, X. Xia, Z. Pang, S. Wang, X. Yu, G. Li, Y. Zhao, Q. Xu, S. Hu, L. Ji, X. Zou and X. Lu, One-step Synthesis of Organic Terminal 2D Ti $_3$ C $_2$ T $_x$ MXene Nanosheets by Etching of Ti $_3$ AlC $_2$ in an Organic Lewis

Acid Solvent, *Angew. Chem., Int. Ed.*, 2024, **63**(23), e202405315, DOI: 10.1002/anie.202405315.

156 H. Shi, P. Zhang, Z. Liu, S. Park, M. R. Lohe, Y. Wu, A. Shaygan Nia, S. Yang and X. Feng, Ambient-Stable Two-Dimensional Titanium Carbide (MXene) Enabled by Iodine Etching, *Angew. Chem., Int. Ed.*, 2021, **60**(16), 8689–8693, DOI: 10.1002/anie.202015627.

157 T. Li, L. Yao, Q. Liu, J. Gu, R. Luo, J. Li, X. Yan, W. Wang, P. Liu, B. Chen, W. Zhang, W. Abbas, R. Naz and D. Zhang, Fluorine-Free Synthesis of High-Purity Ti 3 C 2 T x (T=OH, O) via Alkali Treatment, *Angew. Chem.*, 2018, **130**(21), 6223–6227, DOI: 10.1002/ange.201800887.

158 L. Liang, L. Niu, T. Wu, D. Zhou and Z. Xiao, Fluorine-Free Fabrication of MXene via Photo-Fenton Approach for Advanced Lithium–Sulfur Batteries, *ACS Nano*, 2022, **16**(5), 7971–7981, DOI: 10.1021/acsnano.2c00779.

159 S. Siddique, A. Waheed, M. Iftikhar, M. T. Mehran, M. Z. Zarif, H. A. Arafat, S. Hussain and F. Shahzad, Fluorine-Free MXenes via Molten Salt Lewis Acidic Etching: Applications, Challenges, and Future Outlook, *Prog. Mater. Sci.*, 2023, **139**, 101183, DOI: 10.1016/j.pmatsci.2023.101183.

160 U. Khan, Y. Luo, L. B. Kong and W. Que, Synthesis of Fluorine Free MXene through Lewis Acidic Etching for Application as Electrode of Proton Supercapacitors, *J. Alloys Compd.*, 2022, **926**, 166903, DOI: 10.1016/j.jallcom.2022.166903.

161 M. Li, J. Lu, K. Luo, Y. Li, K. Chang, K. Chen, J. Zhou, J. Rosen, L. Hultman, P. Eklund, P. O. Å. Persson, S. Du, Z. Chai, Z. Huang and Q. Huang, Element Replacement Approach by Reaction with Lewis Acidic Molten Salts to Synthesize Nanolaminated MAX Phases and MXenes, *J. Am. Chem. Soc.*, 2019, **141**(11), 4730–4737, DOI: 10.1021/jacs.9b00574.

162 Y. Li, H. Shao, Z. Lin, J. Lu, L. Liu, B. Duployer, P. O. Å. Persson, P. Eklund, L. Hultman, M. Li, K. Chen, X.-H. Zha, S. Du, P. Rozier, Z. Chai, E. Raymundo-Piñero, P.-L. Taberna, P. Simon and Q. Huang, A General Lewis Acidic Etching Route for Preparing MXenes with Enhanced Electrochemical Performance in Non-Aqueous Electrolyte, *Nat. Mater.*, 2020, **19**(8), 894–899, DOI: 10.1038/s41563-020-0657-0.

163 U. Khan, B. Gao, L. B. Kong, Z. Chen and W. Que, Green Synthesis of Fluorine-Free MXene via Hydrothermal Process: A Sustainable Approach for Proton Supercapacitor Electrodes, *Electrochim. Acta*, 2024, **475**, 143651, DOI: 10.1016/j.electacta.2023.143651.

164 J. Mei, G. A. Ayoko, C. Hu, J. M. Bell and Z. Sun, Two-Dimensional Fluorine-Free Mesoporous Mo2C MXene via UV-Induced Selective Etching of Mo2Ga2C for Energy Storage, *Sustain. Mater. Technol.*, 2020, **25**, e00156, DOI: 10.1016/j.susmat.2020.e00156.

165 N. Xue, X. Li, M. Zhang, L. Han, Y. Liu and X. Tao, Chemical-Combined Ball-Milling Synthesis of Fluorine-Free Porous MXene for High-Performance Lithium Ion Batteries, *ACS Appl. Energy Mater.*, 2020, **3**(10), 10234–10241, DOI: 10.1021/acsaem.0c02081.

166 N. Chen, Z. Duan, W. Cai, Y. Wang, B. Pu, H. Huang, Y. Xie, Q. Tang, H. Zhang and W. Yang, Supercritical Etching Method for the Large-Scale Manufacturing of MXenes, *Nano Energy*, 2023, **107**, 108147, DOI: 10.1016/j.nanoen.2022.108147.

167 A. Numan, S. Rafique, M. Khalid, H. A. Zaharin, A. Radwan, N. A. Mokri, O. P. Ching and R. Walvekar, Microwave-Assisted Rapid MAX Phase Etching and Delamination: A Paradigm Shift in MXene Synthesis, *Mater. Chem. Phys.*, 2022, **288**, 126429, DOI: 10.1016/j.matchemphys.2022.126429.

168 Y. Bai, C. Liu, T. Chen, W. Li, S. Zheng, Y. Pi, Y. Luo and H. Pang, MXene-Copper/Cobalt Hybrids via Lewis Acidic Molten Salts Etching for High Performance Symmetric Supercapacitors, *Angew. Chem., Int. Ed.*, 2021, **60**(48), 25318–25322, DOI: 10.1002/anie.202112381.

169 P. Huang, H. Ying, S. Zhang, Z. Zhang and W. Han, Molten Salts Etching Route Driven Universal Construction of MXene/Transition Metal Sulfides Heterostructures with Interfacial Electronic Coupling for Superior Sodium Storage, *Adv. Energy Mater.*, 2022, **12**(39), 2202052, DOI: 10.1002/aenm.202202052.

170 L. Liu, H. Zschiesche, M. Antonietti, M. Gibilaro, P. Chamelot, L. Massot, P. Rozier, P. Taberna and P. Simon, In Situ Synthesis of MXene with Tunable Morphology by Electrochemical Etching of MAX Phase Prepared in Molten Salt, *Adv. Energy Mater.*, 2023, **13**(7), 2203805, DOI: 10.1002/aenm.202203805.

171 X. Li, M. Li, Q. Yang, G. Liang, Z. Huang, L. Ma, D. Wang, F. Mo, B. Dong, Q. Huang and C. Zhi, In Situ Electrochemical Synthesis of MXenes without Acid/Alkali Usage in/for an Aqueous Zinc Ion Battery, *Adv. Energy Mater.*, 2020, **10**(36), 2001791, DOI: 10.1002/aenm.202001791.

172 M. Shen, W. Jiang, K. Liang, S. Zhao, R. Tang, L. Zhang and J. Wang, One-Pot Green Process to Synthesize MXene with Controllable Surface Terminations Using Molten Salts, *Angew. Chem., Int. Ed.*, 2021, **60**(52), 27013–27018, DOI: 10.1002/anie.202110640.

173 M. Sheng, X. Bin, Y. Yang, Z. Chen and W. Que, A Green and Fluorine-Free Fabrication of 3D Self-Supporting MXene by Combining Anodic Electrochemical In Situ Etching with Cathodic Electrophoretic Deposition for Electrocatalytic Hydrogen Evolution, *Adv. Mater. Technol.*, 2024, **9**(3), 2301694, DOI: 10.1002/admt.202301694.

174 L. Liu, M. Orbay, S. Luo, S. Duluard, H. Shao, J. Harmel, P. Rozier, P.-L. Taberna and P. Simon, Exfoliation and Delamination of Ti $_3$ C $_2$ T $_x$ MXene Prepared *via* Molten Salt Etching Route, *ACS Nano*, 2022, **16**(1), 111–118, DOI: 10.1021/acsnano.1c08498.

175 L. Liu, E. Raymundo-Piñero, P.-L. Taberna and P. Simon, Electrochemical Characterization of Ti3C2T MXene Prepared via a Molten Salt Etching Route in an Acetonitrile-Based Electrolyte, *Electrochem. Commun.*, 2023, **148**, 107453, DOI: 10.1016/j.elecom.2023.107453.

176 Y. An, Y. Tian, Q. Man, H. Shen, C. Liu, S. Xiong and J. Feng, Fluorine- and Acid-Free Strategy toward Scalable

Fabrication of Two-Dimensional MXenes for Sodium-Ion Batteries, *Nano Lett.*, 2023, **23**(11), 5217–5226, DOI: **10.1021/acs.nanolett.3c01201**.

177 X. Zhang, Z. Ni, X. Bai, H. Shen, Z. Wang, C. Wei, K. Tian, B. Xi, S. Xiong and J. Feng, Hierarchical Porous N-doped Carbon Encapsulated Fluorine-free MXene with Tunable Coordination Chemistry by One-pot Etching Strategy for Lithium–Sulfur Batteries, *Adv. Energy Mater.*, 2023, **13**(29), 2301349, DOI: **10.1002/aenm.202301349**.

178 G. Li, L. Tan, Y. zhang, B. Wu and L. Li, Highly Efficiently Delaminated Single-Layered MXene Nanosheets with Large Lateral Size, *Langmuir*, 2017, **33**(36), 9000–9006, DOI: **10.1021/acs.langmuir.7b01339**.

179 L. Huang, T. Li, Q. Liu and J. Gu, Fluorine-Free Ti3C2Tx as Anode Materials for Li-Ion Batteries, *Electrochem. Commun.*, 2019, **104**, 106472, DOI: **10.1016/j.elecom.2019.05.021**.

180 Q. Zhang, J. He, X. Fu, S. Xie, R. Fan, H. Lai, W. Cheng, P. Ji, J. Sheng, Q. Liao, W. Zhu and H. Li, Fluorine-Free Strategy for Hydroxylated Ti3C2/Ti3AlC2 Catalysts with Enhanced Aerobic Oxidative Desulfurization and Mechanism, *Chem. Eng. J.*, 2022, **430**, 132950, DOI: **10.1016/j.cej.2021.132950**.

181 A. A. Mayyahi, S. Sarker, B. M. Everhart, X. He and P. B. Amama, One-Step Fluorine-Free Synthesis of Delaminated, OH-Terminated Ti3C2: High Photocatalytic NOx Storage Selectivity Enabled by Coupling TiO2 and Ti3C2-OH, *Mater. Today Commun.*, 2022, **32**, 103835, DOI: **10.1016/j.mtcomm.2022.103835**.

182 T. Li, X. Yan, L. Huang, J. Li, L. Yao, Q. Zhu, W. Wang, W. Abbas, R. Naz, J. Gu, Q. Liu, W. Zhang and D. Zhang, Fluorine-Free $Ti_3C_2T_x$ (T = O, OH) Nanosheets (~50–100 Nm) for Nitrogen Fixation under Ambient Conditions, *J. Mater. Chem. A*, 2019, **7**(24), 14462–14465, DOI: **10.1039/C9TA03254A**.

183 J. Yoon, S. Kim, K. H. Park, S. Lee, S. J. Kim, H. Lee, T. Oh and C. M. Koo, Biocompatible and Oxidation-Resistant $Ti_3C_2T_x$ MXene with Halogen-Free Surface Terminations, *Small Methods*, 2023, **7**(8), 2201579, DOI: **10.1002/smtd.202201579**.

184 A. Rafieerad, A. Amiri, G. L. Sequiera, W. Yan, Y. Chen, A. A. Polycarpou and S. Dhingra, Development of Fluorine-Free Tantalum Carbide MXene Hybrid Structure as a Biocompatible Material for Supercapacitor Electrodes, *Adv. Funct. Mater.*, 2021, **31**(30), 2100015, DOI: **10.1002/adfm.202100015**.

185 B. Unnikrishnan, C.-W. Wu, A. Sangili, Y.-J. Hsu, Y.-T. Tseng, J. Shanker Pandey, H.-T. Chang and C.-C. Huang, Synthesis and in Situ Sulfidation of Molybdenum Carbide MXene Using Fluorine-Free Etchant for Electrocatalytic Hydrogen Evolution Reactions, *J. Colloid Interface Sci.*, 2022, **628**, 849–857, DOI: **10.1016/j.jcis.2022.07.176**.

186 F. Wang, Z. Bian, W. Zhang, L. Zheng, Y. Zhang and H. Wang, Fluorine-Free MXene Activate Peroxymonosulfate to Remove Tetracyclic Antibiotics, *Sep. Purif. Technol.*, 2023, **314**, 123549, DOI: **10.1016/j.seppur.2023.123549**.

187 N. Xue, X. Li, L. Han, H. Zhu, X. Zhao, J. Zhuang, Z. Gao and X. Tao, Fluorine-Free Synthesis of Ambient-Stable Delaminated Ti_2CT_x (MXene), *J. Mater. Chem. A*, 2022, **10**(14), 7960–7967, DOI: **10.1039/D1TA09981G**.

188 D. Geng, X. Zhao, L. Li, P. Song, B. Tian, W. Liu, J. Chen, D. Shi, M. Lin, W. Zhou and K. P. Loh, Controlled Growth of Ultrathin Mo_2C Superconducting Crystals on Liquid Cu Surface, *2D Mater.*, 2016, **4**(1), 011012, DOI: **10.1088/2053-1583/aa51b7**.

189 C. Xu, L. Wang, Z. Liu, L. Chen, J. Guo, N. Kang, X.-L. Ma, H.-M. Cheng and W. Ren, Large-Area High-Quality 2D Ultrathin Mo2C Superconducting Crystals, *Nat. Mater.*, 2015, **14**(11), 1135–1141, DOI: **10.1038/nmat4374**.

190 T. Thomas, S. Pushpan, J. A. Aguilar Martínez, A. Torres Castro, N. Pineda Aguilar, A. Álvarez-Méndez and K. C. Sanal, UV-Assisted Safe Etching Route for the Synthesis of Mo2CTx MXene from Mo–In–C Non-MAX Phase, *Ceram. Int.*, 2021, **47**(24), 35384–35387, DOI: **10.1016/j.ceramint.2021.08.342**.

191 U. Khan, A. Irshad, L. B. Kong and W. Que, Synthesis of Fluorine-Free Ti3C2Tx MXenes via Acidic Activation for Enhanced Electrochemical Applications, *J. Alloys Compd.*, 2025, **1010**, 177097, DOI: **10.1016/j.jallcom.2024.177097**.

192 M. Ostermann, M. Piljević, E. Akbari, P. Patil, V. Zahorodna, I. Baginskiy, O. Gogotsi, C. Gachot, M. Rodríguez Ripoll, M. Valtiner and P. Bilotto, Pulsed Electrochemical Exfoliation for an HF-Free Sustainable MXene Synthesis, *Small*, 2025, **21**(22), 2500807, DOI: **10.1002/smll.202500807**.

193 F. Tian, F. Wang, W. Nie, X. Zhang, X. Xia, L. Chang, Z. Pang, X. Yu, G. Li, S. Hu, Q. Xu, H. Hsu, Y. Zhao, L. Ji, X. Lu and X. Zou, Tailoring Oxygen-Depleted and Unitary $Ti_3C_2T_x$ Surface Terminals by Molten Salt Electrochemical Etching Enables Dendrite-Free Stable Zn Metal Anode, *Angew. Chem., Int. Ed.*, 2024, **63**(36), e202408996, DOI: **10.1002/anie.202408996**.

194 R. Liu, S. Wei, B. Shi, Y. Ma, L. Sun and W. Wang, Preparation and Properties of Two-Dimensional Ti_2CT_x MXene Based on Electroetching Method, *Nanotechnology*, 2024, **35**(34), 345402, DOI: **10.1088/1361-6528/ad50e2**.

195 Z. Huang, J. Qin, Y. Zhu, K. He, H. Chen, H. Y. Hoh, M. Batmunkh, T. M. Benedetti, Q. Zhang, C. Su, S. Zhang and Y. L. Zhong, Green and Scalable Electrochemical Routes for Cost-effective Mass Production of MXenes for Supercapacitor Electrodes, *Carbon Energy*, 2023, **5**(10), e295, DOI: **10.1002/cey2.295**.

196 F. Yang, Y. Ge, T. Yin, J. Guo, F. Zhang, X. Tang, M. Qiu, W. Liang, N. Xu, C. Wang, Y. Song, S. Xu and S. Xiao, $Ti_3C_2T_x$ MXene Quantum Dots with Enhanced Stability for Ultrafast Photonics, *ACS Appl. Nano Mater.*, 2020, **3**(12), 11850–11860, DOI: **10.1021/acsanm.0c02369**.

197 M. R. Lukatskaya, J. Halim, B. Dyatkin, M. Naguib, Y. S. Buranova, M. W. Barsoum and Y. Gogotsi, Room-Temperature Carbide-Derived Carbon Synthesis by Electrochemical Etching of MAX Phases, *Angew. Chem.*, 2014, **126**(19), 4977–4980, DOI: **10.1002/ange.201402513**.

198 W. Sun, S. A. Shah, Y. Chen, Z. Tan, H. Gao, T. Habib, M. Radovic and M. J. Green, Electrochemical Etching of Ti $_2$ AlC to Ti $_2$ CT $_x$ (MXene) in Low-Concentration Hydrochloric Acid Solution, *J. Mater. Chem. A*, 2017, **5**(41), 21663–21668, DOI: **10.1039/C7TA05574A**.

199 S. Yang, P. Zhang, F. Wang, A. G. Ricciardulli, M. R. Lohe, P. W. M. Blom and X. Feng, Fluoride-Free Synthesis of Two-Dimensional Titanium Carbide (MXene) Using A Binary Aqueous System, *Angew. Chem.*, 2018, **130**(47), 15717–15721, DOI: **10.1002/ange.201809662**.

200 S.-Y. Pang, Y.-T. Wong, S. Yuan, Y. Liu, M.-K. Tsang, Z. Yang, H. Huang, W.-T. Wong and J. Hao, *J. Am. Chem. Soc.*, 2019, **141**(24), 9610–9616, DOI: **10.1021/jacs.9b02578**.

201 Y. Cao, C. Guo and Y. Zou, Rapid Synthesis of MXenes at Room Temperature, *Mater. Sci. Technol.*, 2019, **35**(15), 1904–1907, DOI: **10.1080/02670836.2019.1654250**.

202 T. Yin, Y. Li, R. Wang, O. A. Al-Hartomy, A. Al-Ghamdi, S. Wageh, X. Luo, X. Tang and H. Zhang, Synthesis of Ti3C2Fx MXene with Controllable Fluorination by Electrochemical Etching for Lithium-Ion Batteries Applications, *Ceram. Int.*, 2021, **47**(20), 28642–28649, DOI: **10.1016/j.ceramint.2021.07.023**.

203 J. Chen, M. Chen, W. Zhou, X. Xu, B. Liu, W. Zhang and C. Wong, Simplified Synthesis of Fluoride-Free Ti $_3$ C $_2$ T $_x$ via Electrochemical Etching toward High-Performance Electrochemical Capacitors, *ACS Nano*, 2022, **16**(2), 2461–2470.

204 A. Qian, H. Wu, G. Wang, N. Sun, H. Cheng, K. Zhang and F. Cheng, *ACS Appl. Mater. Interfaces*, 2023, **15**(7), 9203–9211, DOI: **10.1021/acsami.2c19691**.

205 M. Song, S. Pang, F. Guo, M. Wong and J. Hao, Fluoride-Free 2D Niobium Carbide MXenes as Stable and Biocompatible Nanoplatforms for Electrochemical Biosensors with Ultrahigh Sensitivity, *Adv. Sci.*, 2020, **7**(24), 2001546, DOI: **10.1002/advs.202001546**.

206 S.-Y. Pang, W.-F. Io, L.-W. Wong, J. Zhao and J. Hao, Direct and in Situ Growth of 1T′ MoS2 and 1T MoSe2 on Electrochemically Synthesized MXene as an Electrocatalyst for Hydrogen Generation, *Nano Energy*, 2022, **103**, 107835, DOI: **10.1016/j.nanoen.2022.107835**.

207 K. Zheng, X. Zou, X. Xie, C. Lu, S. Li and X. Lu, Electrosynthesis of Two-Dimensional TiC and C Materials from Ti $_3$ SiC $_2$ in Molten Salt, *J. Electrochem. Soc.*, 2018, **165**(5), D190–D195, DOI: **10.1149/2.0651805jes**.

208 Y. A. Kumar, T. Ramachandran, A. Ghosh, A. G. Al-Sehemi, N. P. Reddy and M. Moniruzzaman, A Review on In-Plane Ordered MXenes-Based Materials in Addressing Challenges Faced by Biosensor Applications, *J. Energy Storage*, 2025, **121**, 116507, DOI: **10.1016/j.est.2025.116507**.

209 T. Ramachandran, F. Hamed, Y. A. Kumar, R. K. Raji and H. H. Hegazy, Multifunctional Covalent-Organic Frameworks (COFs)-2D MXenes Composites for Diverse Applications, *J. Energy Storage*, 2023, **73**, 109299, DOI: **10.1016/j.est.2023.109299**.

210 K. V. V. Chandra Mouli, R. M. N. Kalla, T. Ramachandran, Y. A. Kumar, M. Moniruzzaman and J. Lee, Cutting-Edge Advancements in HOFs-Derived Materials for Energy Storage Supercapacitor Application, *Int. J. Hydrogen Energy*, 2024, **90**, 1–24, DOI: **10.1016/j.ijhydene.2024.09.419**.

211 Y. A. Kumar, G. R. Reddy, T. Ramachandran, D. K. Kulurumotlakatla, H. S. M. Abd-Rabboh, A. A. Abdel Hafez, S. S. Rao and S. W. Joo, Supercharging the Future: MOF-2D MXenes Supercapacitors for Sustainable Energy Storage, *J. Energy Storage*, 2024, **80**, 110303, DOI: **10.1016/j.est.2023.110303**.

212 Y. Anil Kumar, S. S. Sana, T. Ramachandran, M. A. Assiri, S. Srinivasa Rao and S. C. Kim, From Lab to Field: Prussian Blue Frameworks as Sustainable Cathode Materials, *Dalton Trans.*, 2024, **53**(26), 10770–10804, DOI: **10.1039/D4DT00905C**.